Geochemistry, Geophysics, Geosystems

RESEARCH ARTICLE
10.1029/2019GC008726

Long Wavelength Progressive Plateau Uplift in Eastern Anatolia Since 20 Ma: Implications for the Role of Slab Peel-Back and Break-Off

Caner Memiş[1], Oğuz H. Göğüş[1], Ebru Şengül Uluocak[2], Russell Pysklywec[3], Mehmet Keskin[4], A.M. Celal Şengör[1], and Gültekin Topuz[1]

[1]Eurasia Institute of Earth Sciences, Geodynamics, Istanbul Technical University, Istanbul, Turkey, [2]Department of Geophysics, Çanakkale Onsekiz Mart University, Canakkale, Turkey, [3]Department of Earth Sciences, University of Toronto, Toronto, Ontario, Canada, [4]Department of Geological Engineering, Faculty of Mines, Istanbul Technical University, Istanbul, Turkey

Key Points:
- Slab peel-back under Eastern Anatolia caused progressive (1.5 km) uplift from north to south
- Plate convergence velocities and plate strength control the magnitude of surface uplift
- Slab break-off may only has a localized effect above the Eurasia-Arabia plate collision zone, not uplifting the entire plateau

Supporting Information:
- Supporting Information S1

Correspondence to:
O. H. Göğüş,
oguzgogus@yahoo.com

Citation:
Memiş, C., Göğüş, O. H., Uluocak, E. Ş., Pysklywec, R., Keskin, M., Şengör, A. M. C., & Topuz, G. (2020). Long wavelength progressive plateau uplift in Eastern Anatolia since 20 Ma: Implications for the role of slab peel-back and break-off. *Geochemistry, Geophysics, Geosystems*, *21*, e2019GC008726. https://doi.org/10.1029/2019GC008726

Received 18 SEP 2019
Accepted 13 JAN 2020
Accepted article online 16 JAN 2020

Abstract Stratigraphic evidence is used to interpret that the East Anatolian Plateau with 2 km average elevation today was below sea level ~20 Ma and uplift began in the northern part. The presence of voluminous volcanic rocks/melt production across the plateau—younging to the south—corroborates geophysical interpretations (e.g., high heat flow and lower seismic velocities) that suggest progressive removal of the slab subducting under the Pontides. Here, we conduct numerical experiments that investigate the change in the surface uplift as a response to slab peel-back and potential break-off processes under subduction-accretionary complexes as well as continental lithosphere. Model results show similar types of tectonic behavior and magnitudes of uplift-subsidence in both oceanic and continental removal processes, and they satisfactorily explain 1.5 km of plateau rise and a ~280 km wide asthenospheric upwelling zone beneath Eastern Anatolia over 18 Myr timescale. Parametric investigation for varying plate strength and convergence velocities show that such model parameters control the amount of surface uplift (1 to 3 km), the width of the asthenospheric upwelling zone, and the potential timing/depth of break-off of the steepening/peeling slab. Experiments show that slab break-off develops during the terminal phase, which may correspond to only a few million years ago. Therefore, the long wavelength plateau uplift and magmatism over the Eastern Anatolian-Lesser Caucasus region since 20 Ma is controlled by progressive slab peel-back and resulting mantle dynamics. The slab break-off process (if it happened) has yet an indiscernible role.

1. Introduction

Geodynamical studies suggest that subducting slabs may peel back from overlying subduction accretionary complexes and continental crust, along weaker lower crust (Bird, 1979; Kimura & Ludden, 1995; Göğüş & Ueda, 2018, and references therein). This delamination-style progressive removal of the lithosphere and associated mantle dynamics suggest a distinct transient migratory pattern of surface subsidence and uplift and magmatism as well as crustal shortening and extension, different from the stationary convective removal process (Houseman et al., 1981; Molnar et al., 1993; Elkins-Tanton, 2007; Göğüş & Pysklywec, 2008b; Wang & Currie, 2015; Göğüş, Pysklywec, Şengör, et al., 2017; Bodur et al., 2018). Such processes of migrating instability mechanism with the surface subsidence and uplift have been linked with various regions: the Colorado Plateau (Bird, 1979; Levander et al., 2011), the Southern Sierra Nevada (Le Pourhiet et al., 2006; Saleeby et al., 2012, 2013), Wallowa mountains-Columbia basalts (Camp & Hanan, 2008; Darold & Humphreys, 2013), Andes (Beck et al., 2015), Southeast Carpathians (Girbacea & Frisch, 1998; Fillerup et al., 2010; Göğüş et al., 2016; van Wyk de Vries et al., 2018; Şengül Uluocak et al., 2019), Apennines (Channell & Mareschal, 1989; Chiarabba & Chiodini, 2013), Alboran Domain-western Mediterranean (Baratin et al., 2016; Docherty & Banda, 1995; Valera et al., 2008), Eastern Anatolia (Keskin, 2003; Şengör et al., 2003, 2008; Göğüş & Pysklywec, 2008a; Göğüş et al., 2011), North Island of New Zealand (Stern et al., 2013), Pamir Mountains (Chapman et al., 2017), and Rhodope-Balkans (Burg, 2011).

We note that the process may be widespread along the Cordilleran and Alpine-Himalayan orogenic belts; nevertheless, there are only a limited number of geodynamic modeling studies—with case-specific focus

—that test the evolution of the ocean and continental slab peeling models against a wide range of geological, geophysical, and petrological observations.

Here, our focus is on the East Anatolian Plateau where abundant evidence for progressive slab removal exists as documented in the subsequent section. Specifically, thermomechanical numerical experiments are used to investigate the geodynamic evolution of Eastern Anatolia and 1.5–2 km of plateau uplift since at least 18 Ma. By building on previous work of Göğüş and Pysklywec (2008a), this parametric numerical study uses new experimental results and recent/updated observations on the geology (e.g., stratigraphy and volcanism) and geophysical data. This provides new insight into the following tectonic problems in Eastern Anatolia and potentially other areas where plate collision and plateau evolution have been suggested:

1. How does the change in model parameters, such as (a) the rheology of the crust, (b) strength of the subducting slab, and (c) the plate convergence velocity control the dynamics and the potential for the slab peel-back and break-off and the resulting mantle upwelling processes?
2. How does surface elevation respond to the impact of progressive slab removal and mantle dynamics?
3. In which parameter ranges are the model results applicable to the geodynamic evolution of Eastern Anatolia (e.g., lithospheric structure, amount-pattern of surface uplift, and possible lower crustal deformation)?

1.1. Geological Background and the Lithospheric Structure of Eastern Anatolia

The East Anatolian high plateau (i.e., the western part of the Turkish-Iranian Plateau) has an average surface elevation of ~2 km and is the highest elevation in the Turkish Syntaxis of the Alpides (Figures 1a and 1b) (Şengör & Kidd, 1979). It is bounded by the Eastern Pontides magmatic arc/Lesser Caucasus Mountains to the north and the Bitlis metamorphic massif to the south (Şengör & Yılmaz, 1981; Yılmaz et al., 1993). The southern margin of the plateau is characterized by active plate convergence between the Eurasian-Arabian lithospheres (to the Zagros), and this collision has been ongoing since at least 20 Ma (Allen et al., 2004; Copley & Jackson, 2006; Dewey et al., 1986; Okay et al., 2010; Yılmaz et al., 1993).

According to Şengör and Yılmaz (1981) and Şengör et al. (2003; 2008), Eastern Anatolia was constructed by tectonic underplating of the subduction-accretionary complex, including Early Jurassic-Late Cretaceous Ophiolitic mélange derived from the Neo-Tethyan ocean lithosphere. These studies emphasize similarities between the tectonic configuration of Eastern Anatolia and the Makran accretionary prism in southeast Iran that developed above the Arabian sea subduction system (Farhoudi & Karig, 1977; Mohammadi et al., 2016; Platt et al., 1985).

Stratigraphic evidence is used to infer that Eastern Anatolia emerged from sea level at least 18 Ma and this surface uplift has not been uniform across the plateau (Figures 2a and 2b). For instance, based on vertebrate fossils findings (e.g., giant rhino *Paraceratherium*, crocodile tooth) within the Late Oligocene-Early Miocene sediments of the Kağızman-Tuzluca basin, Şen et al. (2011) postulates that the northern section of the plateau had already emerged from the sea by then. In the southern section, analysis of foraminiferal assemblages from the Muş basin suggests that the Late Oligocene-Early Miocene (27–22 Ma) was associated with a marine environment (Özcan et al., 2010); moreover, such shallow marine deposition continued until the Serravalian (~13–11 Ma) until the youngest marine regression recorded in the Adilcevaz limestone of the Muş basin (northwest of Lake Van) (Gelati, 1975). This timing was previously considered for the initiation of the surface uplift over the entire plateau (Şengör & Kidd, 1979; Şaroğlu & Yılmaz, 1987; Şengör et al., 2003, 2008). Nevertheless, the stratigraphic correlations across the Eastern Anatolia, Oltu-Balkaya, Kağızman-Tuzluca, Tekman-Karayazı, and Muş basins offer the interpretation that deposition of continental sediments (e.g., gypsum, fluvial and lacustrine clastic rocks, amalgamated with pyroclastics) began in Late Oligocene-Early Miocene in the north, and this progressively migrated to the south during the Middle Miocene (Serravalian) (Sancay et al., 2006; Yılmaz & Yılmaz, 2019).

Corroborating stratigraphic evidence, Erinç (1953) suggests that Miocene-early Pliocene erosion surfaces in the southern part of the plateau (north of the Bitlis suture zone) are dissected by a network of drainage systems (e.g., Euphrates, Figure 2a). In addition, surface uplift of ~800 m has also been inferred by the geomorphological/river incision work along the late Pliocene river terraces in the Murat (a branch of Euphrates) river system (Demir et al., 2009).

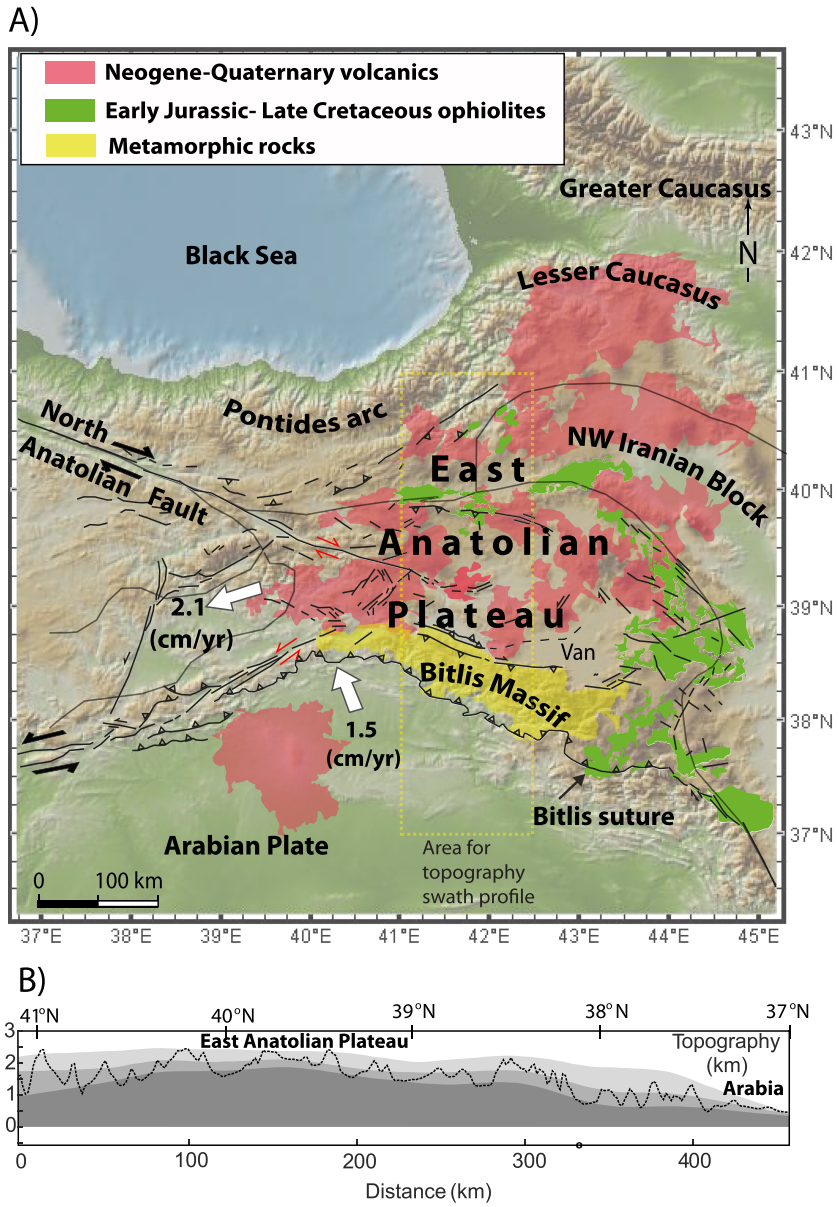

Figure 1. (a) Simplified geological map of Eastern Anatolia region. (b) Dashed rectangle (yellow) represents 150 km wide area N-S topographic swath profiles including minimum, mean, and maximum surface elevations.

The surface geology across the East Anatolian Plateau is dominated by widespread Neogene-Quaternary magmatism approximately (40,000 km^2), varying in composition from basaltic to granitic (Innocenti et al., 1976, 1980, 1982; Pearce et al., 1990; Yılmaz, 1990; Ercan et al., 1990; Notsu et al., 1995; Bigazzi et al., 1997; Keskin et al., 1998; Keskin, 2003, 2007; Şen et al., 2004; Özdemir et al., 2006; Hubert-Ferrari et al., 2009; Kheirkhah et al., 2009; Çolakoğlu & Arehart, 2010; Lebedev et al., 2010; Lebedev, Volkov, et al., 2013; Lebedev, Sharkov, et al., 2016; Lebedev, Chugaev, et al., 2016, Lebedev et al., 2018; Özdemir, 2011; Sumita & Schmincke, 2013; Özdemir & Güleç, 2014; Selçuk et al., 2016; Oyan et al., 2016, 2017; Oyan, 2018; Di Giuseppe et al., 2017; Açlan & Altun, 2018; Rabayrol et al., 2019) (Figures 1a and 2a). These petrological studies infer the lava chemistry, the origin, and the depth of melting in Eastern Anatolia. Although it is not well understood whether there is a clear time-dependent transition from calc-alkaline (subduction related) to alkaline chemistry (decompression melting of the asthenospheric mantle) as originally suggested by Yılmaz (1990) and Keskin (2003) as well as the amount of metasomatized lithosphere that has been

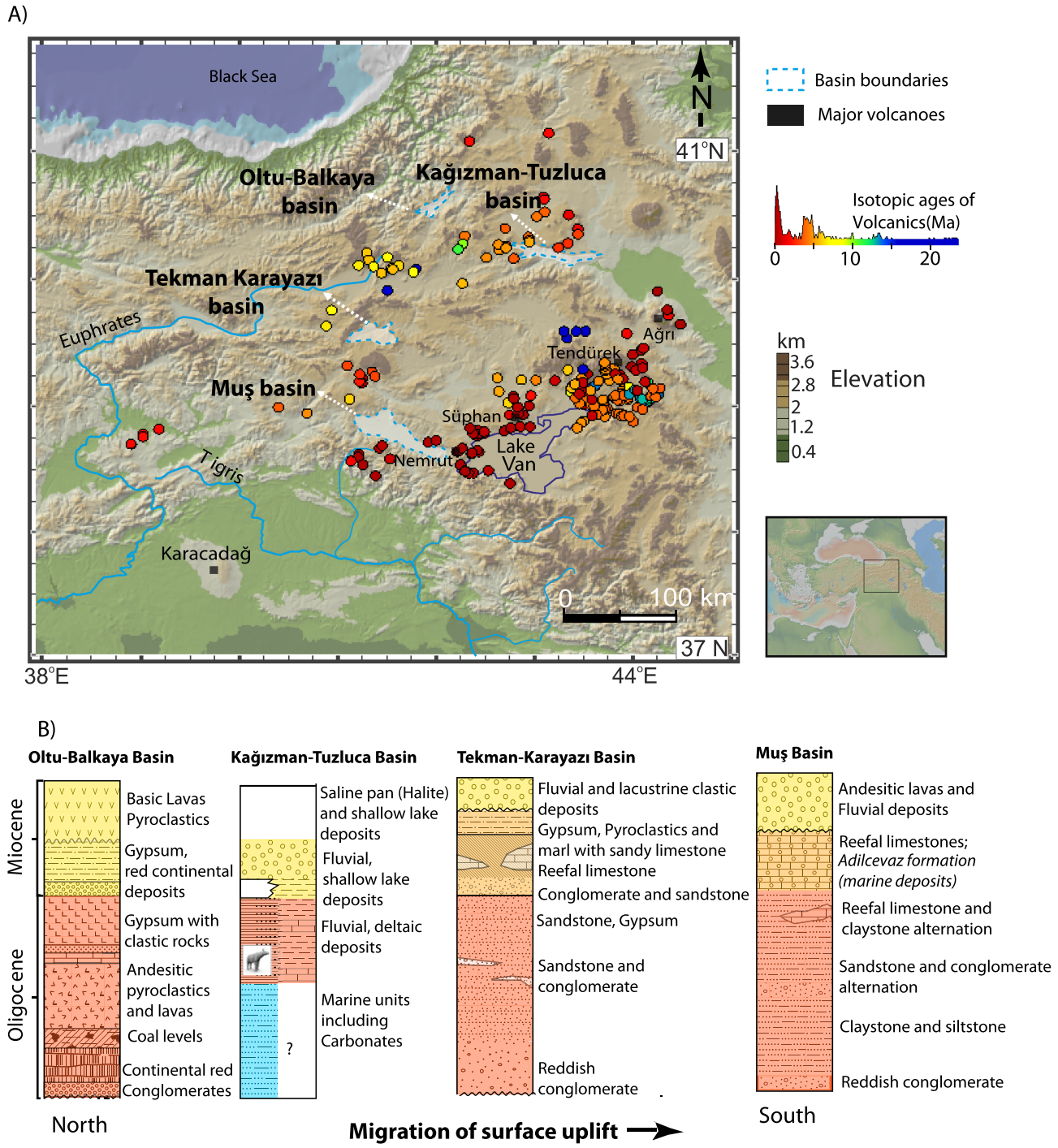

Figure 2. (a) Digital elevation model of the East Anatolian Plateau (GeoMapApp, http://www.geomapapp.org Ryan et al., 2009) showing the major river systems (N-S) cutting across the plateau (Euphrates and Tigris). The Neogene sedimentary basins referred to in this work are also shown in the same figure. Colored dots indicate the isotopic ages of igneous rocks, and the scale bar is included within the same figure frame. (b) Stratigraphic columnar sections of the sedimentary basins (only for Oligocene-Miocene period) are given in sequence from the north (where the surface uplift begins) to the south. The current elevations of these marine sediments are at higher than 1.5 km.

involved with the melting, there is general agreement that the large volume of melt generation under Eastern Anatolia is caused by the high geothermal gradient from an upwelling heat source (e.g., asthenospheric mantle). Independent from their petrological characteristics, a series of isotopic age data from Eastern Anatolian igneous rocks (ranging from 20–0.1 Ma) suggests that older magmatism are

mostly concentrated in the northern part of the plateau whereas the majority of the magmatism (6–4 Ma) occurred in the south around Lake Van, such as Nemrut, Süphan, Tendürek, and Ağrı (see Figure 2a and Table S1 in supporting information for the database). This would suggest that heating and melt production likely had migrated from the north to the south since 20 Ma (Schleiffarth et al., 2018; Rabayrol et al., 2019).

The presence of hot/lower density (asthenospheric) mantle at shallow depths (<100 km) inferred from lower seismic (*P* and *S* wave) velocity anomalies beneath the entire plateau has commonly been interpreted by seismological studies (Hearn & Ni, 1994; Sandvol et al., 2003; Al-Lazki et al., 2003; Piromallo & Morelli, 2003; Maggi & Priestley, 2005; Angus et al., 2006; Gök et al., 2007; Lei & Zhao, 2007; Özacar et al., 2008; Zor, 2008; Gök et al., 2011; Biryol et al., 2011; Mutlu & Karabulut, 2011; Koulakov et al., 2012; Bakırcı et al., 2012; Fichtner et al., 2013; Priestley & McKenzie, 2013; Skobeltsyn et al., 2014; Kind et al., 2015; Delph et al., 2015; Zabelina et al., 2016, Kaban et al., 2018; Portner et al., 2018). Furthermore, seismic tomography models show velocity variations in the mantle that are interpreted to represent slab detachment/break-off under the Bitlis Massif/Arabia-Eurasia plate convergence zone (Bakırcı et al., 2012; Gans et al., 2009; Lei & Zhao, 2007; Mutlu & Karabulut, 2011; Skobeltsyn et al., 2014; Zor, 2008). The high heat flow estimates corroborate relatively shallow Curie-point depth measurements (~ < 20 km) (Ates et al., 2005) and surface heat flow anomalies from volcanic rocks (up to 85–90 mW/m^2) (Tezcan, 1995). Based on geochemical analysis of basaltic rocks and the inversion from the seismic tomography model of Priestley and McKenzie (2013), recent work by McNab et al. (2018) agrees well with inferences of hot asthenospheric mantle residing as shallow as 60 km depth under East Anatolia, where mantle potential temperatures reach ~1400°.

These geological, geophysical, and petrological studies collectively suggest that the southward migration of surface uplift (>1.5 km) and melt production/volcanism across the East Anatolian Plateau is primarily controlled by hot asthenospheric mantle flow entering from the north to the south since ~20 Ma, presumably by the peel-back of the subducting slab from the overlying shortening crust. Previous conceptual models by Şengör et al. (2008) and Keskin (2003, 2007) made an attempt to explain the geodynamic origin of plateau growth and volcanism by the peeling (steepening) and the break-off (during the later stages) of the Neotethyan oceanic slab from the subduction-accretionary complex, accompanied by opening out an asthenospheric mantle wedge gradually widening to the south in time.

Here, we also test quantitatively if and how much slab break-off plays a role during the evolution of progressive slab removal for the 18 Myr lithospheric evolution of Eastern Anatolia. A set of numerical experiments also considers the influence of continental crust rheology—as an alternative to the subduction accretionary crust—for the plateau evolution in Eastern Anatolia.

2. Model Design

2.1. Model Descriptions and Geological Preconditions for Slab Peeling Under Eastern Anatolia

Figures 3a and 3b and Table 1 illustrate the initial geometry and physical parameters (e.g., densities, temperature field, and length scales) used in the reference slab peeling experiments for the ocean (EXP-1, Figure 3a) and continental lithosphere (EXP-2, Figure 3b). The model domain is 2,000 km wide and 660 km deep. This depth represents the upper-lower mantle transition where the penetration of the slab beneath this boundary is not considered. The initial setup is designed as an approximately N-S, (NNE, SSW) cross section through Eastern Anatolia, orthogonal to the plate boundary in the south (the Arabia-Eurasia collisional zone).

The model configuration is approximated to represent the tectonic state of the region 20–18 Myr ago when the lithospheric slab was ready to peel back from the overlying crust. The experiments that test ocean lithosphere peeling from the overlying accretionary complex consider that the removal begins following the subduction of the northern branch of Neo-Tethys under the Pontides. Such a subduction process under the Rhodope-Pontide fragment has been active since at least the Late Eocene (Keskin, 2003, 2007; Şengör et al., 2003, 2008; Topuz et al., 2011). Alternative experiments with continental mantle lithosphere and lower crust peeling (delaminating) from the overlying (upper-middle) continental crust consider that such lithospheric gravitational instability/shortening began as a response to the Miocene Arabia-Eurasia plate collision (18–13 Ma) at the southern border of the East Anatolian plateau (Cavazza et al., 2018; Okay et al., 2010).

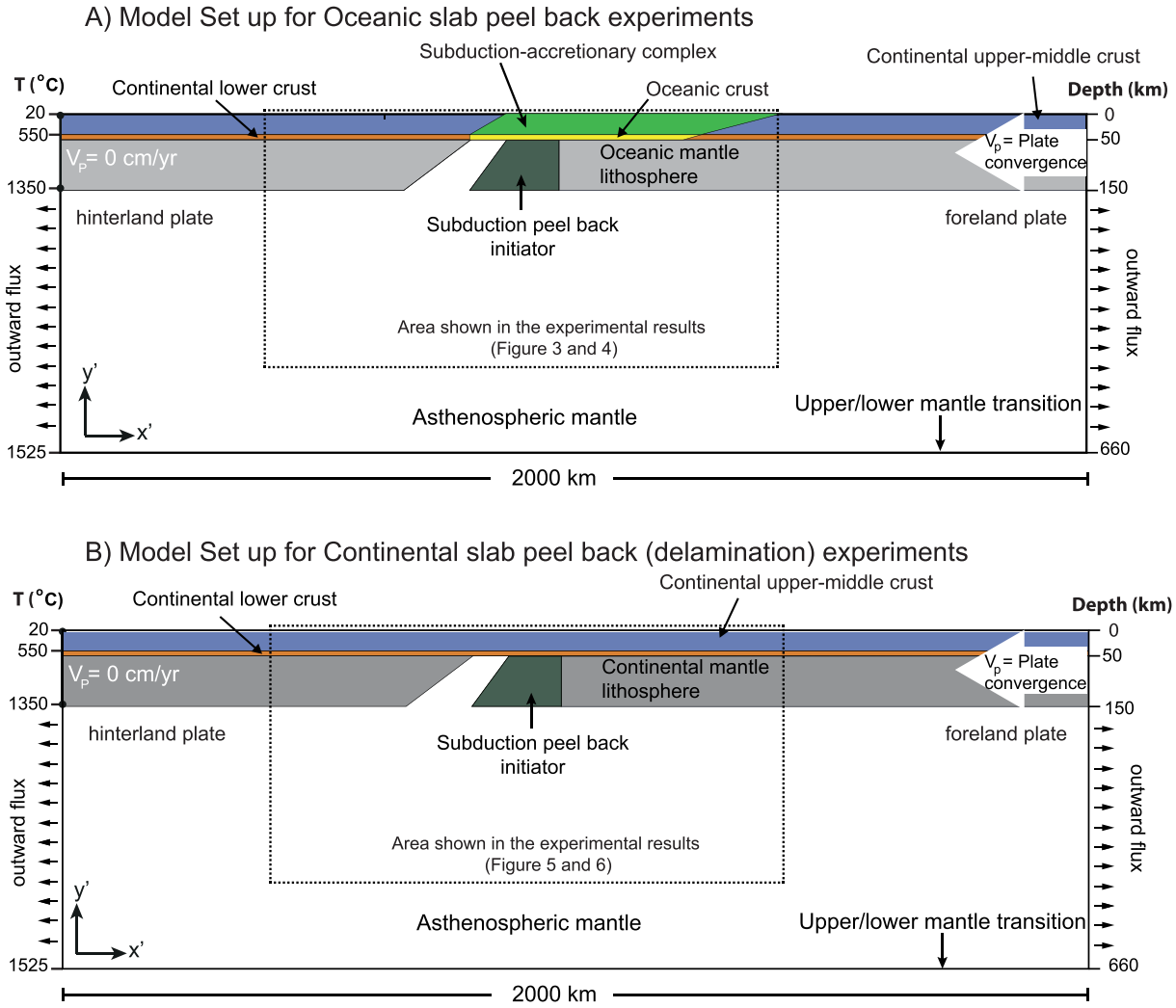

Figure 3. Illustration of experiment design for (a) oceanic slab peel-back from the accretionary crust and (b) continental slab peel-back (delamination) experiments, including model geometry, boundary conditions, and initial temperature at the base of each layer (Please see Table 1 for major rheological parameters and material properties used in the numerical experiments). The experimental setup is an approximation to the N-S, NE-SW cross-section (from Bitlis massif to the Eastern Pontides/Lesser Caucasus) across Eastern Anatolia. The convergent plate velocity is imposed on the right side of the lithosphere ($V_P = 2$ cm/year), an approximation to the GPS-derived plate velocity (Reilinger et al., 2006). To keep the mass conserved, the injected amount of material volume is taken out of the solution box beneath the foreland and hinterland lithospheres, evenly along from both left and right margins of the model box.

Figure 3a shows the initial design for the oceanic lithosphere peeling model domain in which the following layers are described from the top to bottom. At the very top and in the middle section, there is 40 km thick and 500 km wide subduction accretionary complex (mafic composition), defined by Maryland diabase rheology (light green colored; Mackwell et al., 1998). Meanwhile, continental crust (wet quartzite rheology) (Gleason & Tullis, 1995), shown in dark blue, is used for the rest of the model domain, and it represents the continental basement rocks of the Bitlis Massif to the south and the Pontide continental magmatic arc to the north. The accretionary complex is underlain by 10 km thick oceanic crust as diabase rheology (yellow colored; Ranalli, 1997); beneath this, there is 100 km thick oceanic mantle lithosphere, with dry olivine rheology (gray; Hirth & Kohlstedt, 1996). These are all underlain by asthenospheric mantle that has a dry olivine rheology at the bottom (white; Hirth & Kohlstedt, 1996).

Figure 3b shows the setup for the reference continental lithosphere (mantle lithosphere and lower crust) peeling (delamination) experiment. The model domain includes 40 km thick upper-middle continental crust, wet quartzite rheology (dark blue; Gleason & Tullis, 1995). The upper-middle crust is set to be relatively thicker in these experiments because it is designed to represent the evolution of an active orogenic

Table 1
Rheological Parameters, Material Properties Including (Density, Temperature) for the Ocean Slab (EXP-1) and Continental Slab Peel-Back (Delamination) (EXP-2) Reference Experiments

	Oceanic lithosphere		Continental lithosphere			
Model Parameters	Accretionary complex	Oceanic crust	Upper crust	Lower crust	Mantle lithosphere	Asthenosphere
Reference density (ρ_0, kg/m^3)	2,900	3,000	2,840	2,990	3,300	3,260
Internal angle of friction (ϕ)	15–2°	15–2°	15–2°	15–7°	0	0
Power law exponent (n)	4.7	3.4	4	3.1	3.5	3.5
Viscosity parameter (A, Pa^{-n}/s)	5.04×10^{-28}	2×10^{-24}	1.1×10^{-28}	8×10^{-23}	4.89×10^{-17}	4.89×10^{-17}
Plastic yield stress (C_M/C_C, MPa)	1	0	1	0	75	0
Activation energy (Q, kJ/mol)	485	260	223	243	515	515
Heat capacity (C_p, J·kg^{-1}·K^{-1})	770	773	793	793	793	793
Thermal expansion coefficient (α, K^{-1})	2×10^{-5}	3×10^{-5}	2×10^{-5}	3×10^{-5}	2×10^{-5}	2×10^{-5}
Rheology	Dry maryland diabase	Diabase	Quartz	Felsic granulite	Olivine	Olivine
Reference	Mackwell et al. (1998)	Ranalli (1997)	Gleason and Tullis (1995)	Mackwell et al. (1998)	Hirth and Kohlstedt (1996)	Hirth and Kohlstedt (1996)

Note. See the text for detailed explanations.

zone where plate convergence (crustal shortening) has been ongoing since at least by the Early-Middle Miocene, ~18–13 Myr ago (Okay et al., 2010). Such 50 km thick crust in total is an approximation to the central Alps plate convergence (Yan & Mechie, 1989), although our lower crust is 10 km thinner here. The upper-middle crustal layer is underlain by 10 km thick lower crust of felsic granulite rheology (orange; Ranalli, 1997). The continental crust is underlain by 100 km thick continental mantle lithosphere, and this is represented by dry olivine rheology (light gray; Hirth & Kohlstedt, 1996). The mantle lithosphere is underlain by the asthenospheric mantle down to the bottom of the solution box and also has the dry olivine rheology (white; Hirth & Kohlstedt, 1996).

The rheological and other main model parameters for both oceanic and continental lithospheric slab experiments are given in Table 1. The laboratory-based rheological parameters used in this and other numerical modeling studies may be associated with significant uncertainties owing to the varying water content or the limited number of samples in individual rock selection (Beaumont et al., 2006; Currie et al., 2008; Göğüş et al., 2016; Gray & Pysklywec, 2012; Huismans & Beaumont, 2008; Pysklywec et al., 2002). The power law viscous parameters for the subduction accretionary complex are selected as Maryland diabase rheology (Mackwell et al., 1998). This is because East Anatolia (accretionary) crust inherently would constitute oceanic material (ophiolites including cumulate gabbros and ultramafics), and estimates from generic study suggest that more than 50% sediments entering into the subduction accretion systems may tectonically be eroded (von Huene & Scholl, 1991) while leaving over more mafic crust. Meanwhile, we scaled down the effective viscosity of this layer by a factor of 0.1 to approximate the properties of weak crust/accreted ocean material, made up of flysch deposits, ophiolitic mélanges, and fragmented limestone blocks. Given the uncertainties of the rheological parameters (A, n, ρ, Table 1), the reduction of viscosity by a factor 10 is an arbitrary selection for the accretionary complex, but this may be an approximation for the highly deformed rocks under hydrated conditions.

The initial density of the oceanic mantle lithosphere is chosen to be 40 kg/m^3 higher than the underlying asthenospheric mantle to facilitate the slab instability and evolving peeling process. According to the integrated petrological and geophysical modeling work by Afonso et al. (2007), $\Delta\rho = 35$ kg/m^3 is in reasonable range inferred by the depth averaged calculations for 90 Ma old ocean lithosphere. Schubert et al. (2001) suggests that such a difference can be as high as $\Delta\rho = 70$ kg/m^3. A range of experiments with decreased and increased density differences are also conducted, but 40 kg/m^3 is set to fine tune for the timing of the initiation of uplift and magmatism in Eastern Anatolia over the last ~20–18 Myr.

On the other hand, for the continental mantle lithosphere peeling (delamination) under Eastern Anatolia, there is a strong possibility that the deeper levels of the lower crust and the upper parts of the mantle lithosphere may be densified through eclogizitation due to plate collision and shortening (Leech, 2001) and/or metasomatization by fluid infiltration through flux melting of the arc

magmatism in relation to the Neo-Tethys subduction of the Arabian plate in the south (Chin et al., 2014; Le Roux et al., 2007).

In our experiments, the lithospheric removal process begins when 100–150 km wide and 100 km thick gravitationally unstable ocean lithosphere (ρ_0 = 3,400 kg/m^3, dark green) starts to sink into the sublithospheric mantle. This is a physical approximation for the presence of steep and sufficiently dense slab subducting under the Rhodope-Pontide fragment (e.g., similar to Japan) as hypothesized by Okay and Şahintürk (1997) that initiates the peel-back of the slab ~18 Ma (Şengör et al., 2008). To represent the Eurasian-Anatolian plate boundary as a lithospheric scale shear zone, a conduit of asthenospheric mantle (low viscosity-weak zone) is inserted to allow for the upwelling of the asthenospheric mantle that facilitates the removal process (Bird, 1979; Göğüş & Pysklywec, 2008b; Göğüş, Pysklywec, & Faccenna, 2017).

2.2. Boundary Conditions and Temperature Field

The numerical resolution is 201 × 101 (width and depth) Eulerian nodes and 601 × 301 Lagrangian nodes. Half of the Eulerian and Lagrangian elements are concentrated in the top 150 km in order to enhance resolution in the uppermost lithosphere. The model has a free top surface, allowing topography to develop as the model evolves. No material flux is allowed through the bottom boundary, but varying plate velocities are imposed on the margins in the horizontal direction to approximate plate convergence (e.g., V_P = 1–3 cm/year). The velocity boundary conditions are described as a constant inflow from the top to 150 km depth at the right boundary with constant outflow imposed from beneath the lithosphere down to 660 km depth through both sides. The magnitude of the outflow equals the volume of inflow to conserve the mass in the model domain. The lithosphere on the left margin is held fixed (pinned) for all model experiments.

The initial geotherm for the experiments is laterally uniform and is defined by a surface temperature of 20 °C, an increase to 550 °C at the Moho, an increase to 1350 °C at the base of the mantle lithosphere and an increase to 1525 °C at the bottom of the model (Figure 3). The surface and bottom temperatures are held constant throughout the experiments and the heat flux across the side boundaries is 0. The initial temperature profile is the same in all experiments.

2.3. Governing Equations

Numerical calculations are carried out by the SOPALE numerical software that uses arbitrary Lagrangian-Eularian finite element techniques to solve for the plane strain deformation of complex viscoplastic behavior of materials (Fullsack, 1995). This technique is useful for treating finite deformations, and for tracking boundaries such as free surface and motion of internal particles at any depth (Fullsack, 1995; Göğüş & Pysklywec, 2008b). Numerical experiments consider 2-D incompressible flow, and the governing equations for thermomechanical behavior includes conservation of mass, momentum, and internal energy. This is described as

$$\nabla(\rho u) = 0 \tag{1}$$

$$\nabla(\sigma_{ij}) + \rho g = 0 \tag{2}$$

$$\rho C_{\mathrm{p}}\left(\frac{\partial T}{\partial t} + u{\cdot}\nabla T\right) = k\nabla^2 T + \rho H \tag{3}$$

The equation of state is given by

$$\rho = \rho_0[1{-}\alpha(T{-}T_0)] \tag{4}$$

In equations (1)–(4), ρ, T, and u represent density, temperature, and velocity, respectively. Likewise, g, α, H, and t are variables symbolizing gravitational acceleration (m^2/s), thermal expansivity (K^{-1}), rate of internal heat production per unit mass (W/kg), and time respectively. Thermal conductivity (k = 2.25 W·m^{-1}·K^{-1}) is the same for all materials, and we ignore radioactive heat production, erosion, and shear heating in the models (e.g., Göğüş & Pysklywec, 2008b, see Table 1).

The stress tensor in equation (2) includes two components as follows:

$$\sigma_{ij} = \sigma'_{ij} - P\delta_{ij} \tag{5}$$

where σ'_{ij} represents deviatoric stress tensor and P is pressure (in case of an incompressible fluid, $P = -\frac{1}{3}\sigma_{ii}$). It is also important to note that viscoplastic deformation of the grids is executed at the lesser value of either a yield stress (σ_{yield}) or viscous stress ($\sigma_{viscous}$) for each computation. This relation can be shown below:

$$\sigma'_{ij} = \min\left(\sigma_{yield}; \sigma_{viscous}\right) \tag{6}$$

A Drucker-Prager yield law is used for frictional plastic yield stress, similar to the Coulomb criterion in plane strain (Beaumont et al., 2006; Fullsack, 1995):

$$\sigma_{yield} = P\sin\phi + c_o \text{ (crust)} \tag{7}$$

$$\sigma_y = C_m \text{ (mantle)} \tag{8}$$

where c_o is cohesion. For the crust, an empirical weakening with the internal angle of friction varying dependent on the strain from ϕ = 15–7°. Here, ϕ = 15° is an effective internal angle of friction that implicitly includes the effects of pore fluid pressure in the crust. This is a conventional approach in these types/scales of numerical modeling (e.g., Gray & Pysklywec, 2012; Pysklywec et al., 2010) in which critical Coulomb wedge studies by Dahlen et al. (1984) suggest ϕ = 15° for the rocks in the fold-thrust belt of the western Taiwan. The crustal weakening employed in these models takes into account the shear zone related deformations (e.g., cataclastic flow, fault gouges) (Beaumont et al., 1996).

The equation for viscous stress is

$$\sigma_{viscous} = 2\eta_e\dot{\epsilon} \tag{9}$$

where the effective viscosity (η_e) of the materials for power law rheology is defined as

$$\eta_e(\dot{\epsilon}, T) = GA^{\frac{-1}{n}}\dot{\epsilon}^{\frac{1-n}{n}}e^{\frac{Q}{nRT}} \tag{10}$$

The variables $\dot{\epsilon}$, A, Q, n, and R represent strain rate (s^{-1}), viscosity parameter (Pa^{-n}/s), activation energy from uniaxial laboratory experiments (kJ/mol), power law exponent, and ideal gas constant, respectively. G is a parameter required for the conversion of the uniaxial laboratory data to a condition of stress, which is not dependent on the coordinate system (Pysklywec et al., 2002):

$$G = \left(3^{\frac{-(n+1)}{2n}}2^{\frac{(1-n)}{n}}\right) \tag{11}$$

3. Experimental Results

Numerical experiments investigate the surface response to the slab peeling and (break-off) from beneath, subduction-accretionary complex, and the continental crust. The work is carried out as a parametric numerical study that included a series set of geodynamical experiments. While the impact of plastic yield stress/strength and plate convergence velocities are tested, below we only explain the selected experimental results that relate to the Eastern Anatolia's plateau development.

3.1. Ocean Lithosphere Peel-Back Model (EXP-1) (σ_y = 75 MPa, V_P = 2 cm/year)

Figures 4a–4c show the geodynamic evolution of the oceanic lithosphere peel-back model (EXP-1) and associated surface topography/crustal thickness variations for 10, 14.5, and 18 Myr from the beginning of the experiment. The plate convergence velocity (V_P = 2 cm/year) imposed on the right side of the lithosphere margin is a close approximation to the inferred plate velocity of the northward motion of the Arabian plate (Reilinger et al., 2006). The descending oceanic lithosphere deforms under σ_y = 75 MPa plastic yield stress (e.g., an arbitrary selection) and it breaks off when it reaches such a mechanical condition.

After 10 Myr since the initiation of the experiment (Figure 4a), the oceanic lithosphere subducts into asthenospheric mantle, meanwhile it has peeled back under the overlying subduction-accretionary complex

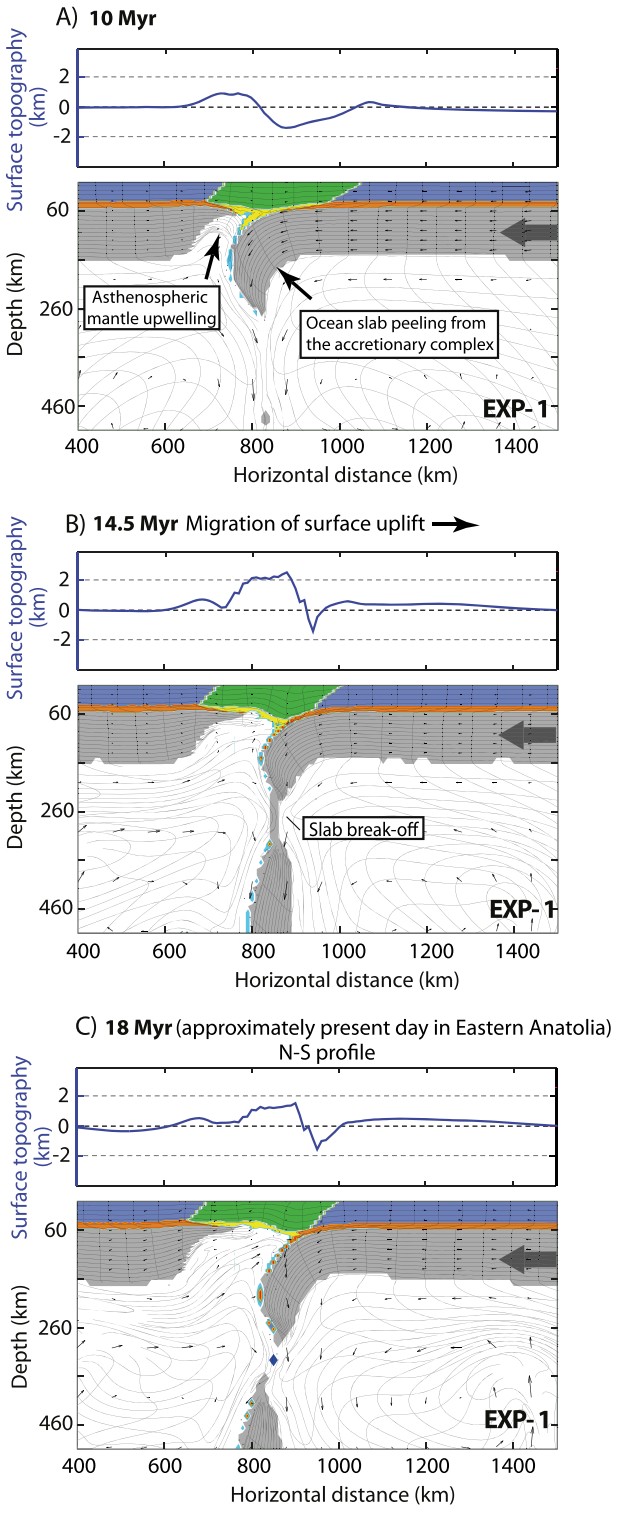

Figure 4. Geodynamic evolution of the reference/preferred experiment (EXP-1) demonstrating the slab peel-back and break-off from beneath the accretionary crust in Eastern Anatolia. These plots show such evolution at (a) 10, (b) 14.5, and c) 18 Myr after the beginning of the experiment. The plots above the geodynamic model/lithospheric structure show the change in the surface topography plotted for each time, respectively.

(green color) along the weak oceanic crust (yellow color), which acts as a decoupling layer between the two. The model timing for 10 Myr may approximately correspond to 8–10 Ma in Eastern Anatolia when surface uplift and volcanism occurs (e.g., Erzurum-Kars plateau) under the north central section of the plateau (Keskin, 2003, 2007; Keskin et al., 1998; Şen et al., 2011; Şengör et al., 2008). The surface expression of such slab peeling at this stage is represented by positive (up to 1 km) and negative (down to −1 km) surface topography variations that include both the isostatic and dynamic effects. For the surface uplift, the isostatic response operates as a consequence of the replacement of less dense asthenospheric mantle with the denser mantle lithosphere and crustal shortening imposed by plate convergence. At the same time, there is dynamic topography due to the vertical stresses induced by asthenospheric mantle flow (Braun, 2010).

After 14.5 Myr, following to the slab steepening up to 90° dip angle, the hanging slab is almost broken off from the rest (partially attached to the overlying lithosphere), while necking at depths of 200–300 km. More lithospheric material has peeled back from beneath the accretionary crust by now, and consequently there is a broader region of positive surface topography (Figure 4b). A surface elevation of +2 km is attained along this plateau type >100 km wide area. At the same time, there is surface subsidence on the margin of the plateau, again due to the (partially attached) slab pulling the crust down. Owing to the same effect, there the crust thickens significantly where the slab and the overlying accretionary material is separated or decoupled. In this study we refer to this position as the "decoupling hinge," similar to the migrating hinge at the retreating ocean subduction systems between the ocean and continental plate.

Following to the complete slab detachment at 18 Myr (i.e., approximately present-day Eastern Anatolia), both the geodynamic configuration of the model and its surface/crustal manifestation does not change considerably compared to 14.5 Myr. For instance, plateau like surface topography, 1.5 km high still prevails across slab peel off zone (Figure 4c).

At the final stage, this experiment predicts surface topography variation (viz., a plateau and adjacent localized subsidence) as well as (deep) lithospheric configuration, comparable to the tectonic evolution of Eastern Anatolia. Specifically, the ocean slab peeling and the resulting mantle replacement zone corresponds to the seismologically inferred low velocity zone under the East Anatolian plateau and a piece of detached slab shown in several seismic tomography models (see section 5 for comparison between models).

3.2. Variations in the Strength of the Oceanic Mantle Lithosphere (σ_y = 60, 90 MPa)

The large-scale (plateau-wide) effect of the slab break-off process under the southern margin of the East Anatolian plateau is investigated with varying plastic yield stresses of the mantle lithosphere. A range of experiments with σ_y = 30–120 MPa were conducted (while all other parameters were taken same with the reference experiment EXP-1). Here we show the evolution of two representative models in which the plastic yield stress was set to σ_y = 60 MPa for the EXP-OC62 (lower strength compared to EXP-1) and σ_y = 90 MPa for EXP-OC92 (higher strength compared to EXP-1).

Figure 5a for EXP-OC62 shows the geodynamic evolution and associated surface topography-crustal thickness variation of this experiment at 10 and 18 Myr. During the earlier stages, this model develops similar to EXP-1. For example, by 10 Myr, the heavy piece of slab has already detached from the rest of the lithosphere, slightly dipping into the mantle. As in the previous model, the positive surface elevation (less than 1 km) is induced by mantle rising under the crust. By 18 Myr, (only 1 Myr after the slab break-off), the replacement of hot upwelling mantle with cold/dense mantle lithosphere in the removal zone increases the elevation (~2 km) and the sinking slab creates surface depression adjacent to the flat and high (plateau) surface topography area.

In EXP-OC92 with stronger ocean mantle lithosphere, the slab peeling process evolves slightly more rapidly (Figure 5b). For instance, at 10 Myr, there is more oceanic slab (including crust) sinking into the mantle compared to EXP-1 and EXP-OC62. This more intact/steep slab inherently creates a larger amount of downward forcing than these other two experiments for 10 Myr. Namely, a negative surface deflection (up to −2 km) develops as a response to such downwelling process (Figure 5b). By 18 Myr, unlike EXP-1 and EXP-OC62, the slab break-off does not develop. Rather a continuous folded slab touches the bottom of the solution box at 660 km. Even without a slab break-off, the zone of positive surface topography including the plateau type (1.5 km high) region (x = 800–950 km) still develops as a consequence of the lithosphere peeling and related asthenospheric mantle uprising. This suggests that both slab break-off and simple peeling/delamination without break-off processes could lead to relatively longer wavelength surface uplift of East Anatolia.

3.3. Continental Lithosphere Peel-Back/Delamination Model (σ_y = 75 MPa, V_P = 2 cm/year)

Figures 6a–6c shows the geodynamic impact of peeling back of the continental mantle lithosphere from beneath the continental crust and the surface response to it (EXP-2). This model is an approximation in the (sensu stricto) to continental delamination as defined by Bird (1979) for the uplift of the Colorado Plateau. Here, numerical experiments test the predictions of a similar mechanism for the continental setting rather than ocean subduction models discussed above. In order to make the sensible comparison against the ocean lithosphere experiments, model parameters remained the same with EXP-1.

EXP-2 at Figure 6a shows that by 10 Myr, the delamination progresses and migration of the paired uplift and subsidence of surface topography pattern persists. The development of such process is slightly (~0.5 Myr) more rapid in the continental lithosphere experiments until 14.5 Myr, compared to oceanic slab removal models (Figures 4b and 4c). The model is represented by positive surface topography (nearly 1 km maximum surface uplift) and surface depression where the slab is subducting and pulling the crust.

By 14.5 Myr, domal surface topography develops with maximum elevation exceeding 2 km at ~ x = 800 km. Specifically, the surface elevation gradually increases from 0 at x = 600 km to the peak elevation and then decreases to 0 at x = 900 km (Figure 6b).

At 18 Myr, the lithospheric slab has peeled further from the continent and the detached slab has reached mantle depths >500 km (Figure 6c). Note that for the same time, the ocean lithosphere model shows that there is descending slab at depths of 300–460 km. The comparison between EXP-1 and EXP-2 suggests that more buoyant continental crust promotes the increasing pace of lithospheric removal and break-off, although it is not significant. For the continental setting, the migrating, wave-like pattern of surface topography show similarities with the ocean lithosphere peeling back model, in which >1.5 km of surface uplift develops (>100 km wide). This is as a response to the mobilization of the underlying slab. Though not overly distinct and obvious, surface elevation profiles for the ocean and the continental peel-back models suggest that for the continents the surface rise is not necessarily restricted to the area where the slab is peeling back. Rather, the uplift disseminates to broader areas, most likely because of the homogenous distribution of the crustal rheology along the model domain.

3.3.1. Variations in the Strength of the Continental Mantle Lithosphere (σ_y = 60, 90 MPa)

A series of models tested different plastic yield stress for the mantle lithosphere (σ_y = 30–120 MPa), where otherwise the rest of the model parameters are identical to the preferred experiment for the continental setting (EXP-2). As representative models, Figure 7a shows the evolution of EXP-62 with weaker continental mantle lithosphere rheology (plastic yield stress is set to σ_y = 60 MPa) and EXP-92 has stronger mantle lithosphere rheology with σ_y = 90 MPa (Figure 7b).

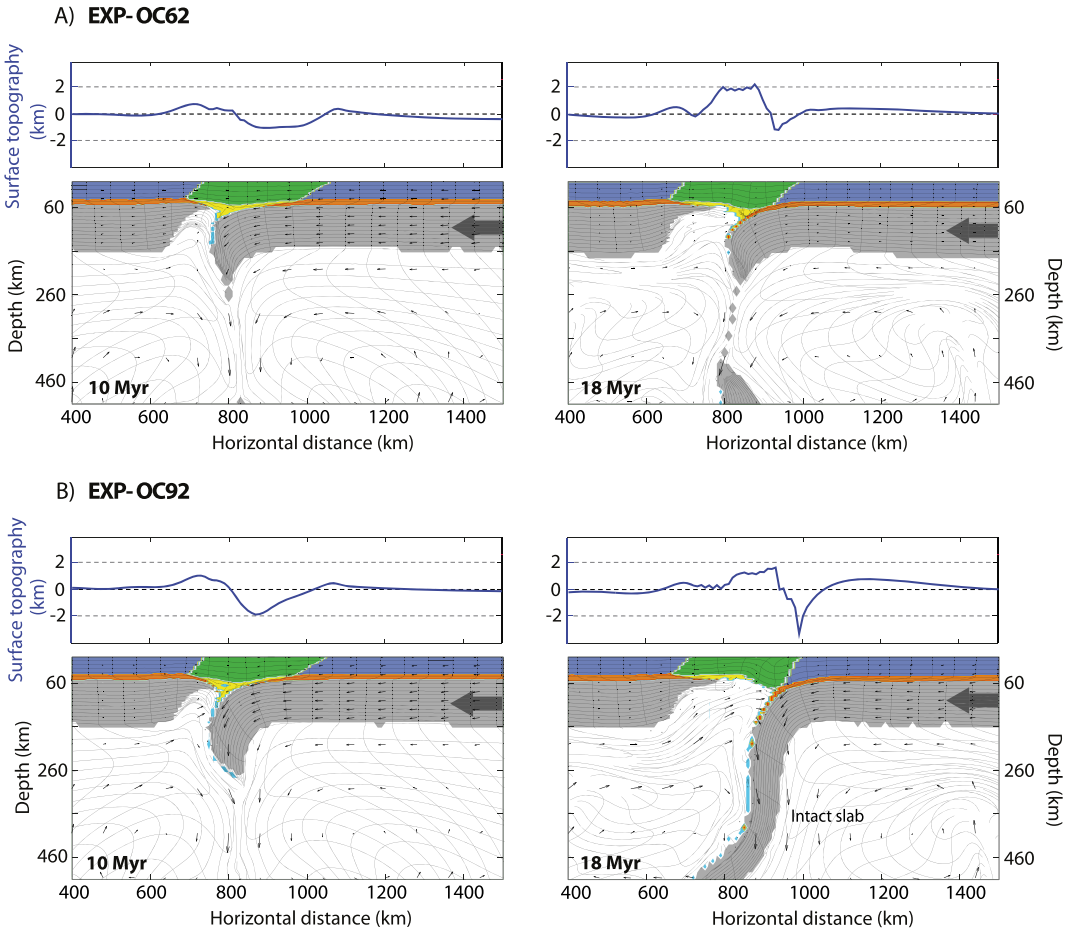

Figure 5. Geodynamic evolution of experiments; (a) EXP-OC62, and (b) EXP-OC92. The only difference between these two experiments is the plastic yield stress of the oceanic lithosphere, set initially as $\sigma_y = C_m$ (mantle). $\sigma_y = 60$ MPa of plastic yield stress is used for experiment EXP-OC62 (weaker rheology), while $\sigma_y = 90$ MPa is used for EXP-OC92 (stronger rheology). All other parameters are identical to the reference experiment (EXP-1). Both experiments show the model configuration for 10 and 18 Myr after the beginning of the experiment. Accordingly, surface topography profiles plots are shown on top of each panel for the relevant time frame.

For EXP-62, at 10 Myr, there is relatively less lower crust and mantle lithosphere descent into the mantle and the associated surface subsidence is less compared to EXP-2. Meanwhile, the positive surface topography is comparable to EXP-2 because of the mantle uprising underneath the crust. At 18 Myr, the slab just breaks off, and it is delayed for a few million years because there is less plate bending during slab peel-back from the crust with weaker lithosphere rheology. Such weaker lithosphere rheology is associated with the earlier removal of the preexisting denser slab piece (see setup for the details); therefore, it causes the reduction of slab pull forcing which promotes bending and sinking of the lithosphere into the mantle. Owing to the response to a recent slab break-off, the surface elevation maxima of >2 km is attained (Figure 7a). Nevertheless, this has a localized domal type surface high (shorter wavelength), rather than a wider (longer wavelength) plateau type elevation.

With the stronger continental mantle lithosphere rheology in EXP-92 (Figure 7b) the model results are similar to EXP-2 and the slab breaks off (maximum stretching of the lithosphere) about the same time, 15 Myr (just 0.5 Myr later). When compared EXP-62 (Figure 7a) to EXP-92 (Figure 7b), there is 3 Myr difference in the slab break-off time, which shows how relatively even smaller amount of plate strength difference can control the timing of the process. As with the ocean lithosphere models, the stronger lithospheric slab bends and peels back more, allowing for a broader zone of mantle upwelling. There are differences between the continental versus oceanic ocean slab peeling experiments when the mantle lithosphere rheologies are

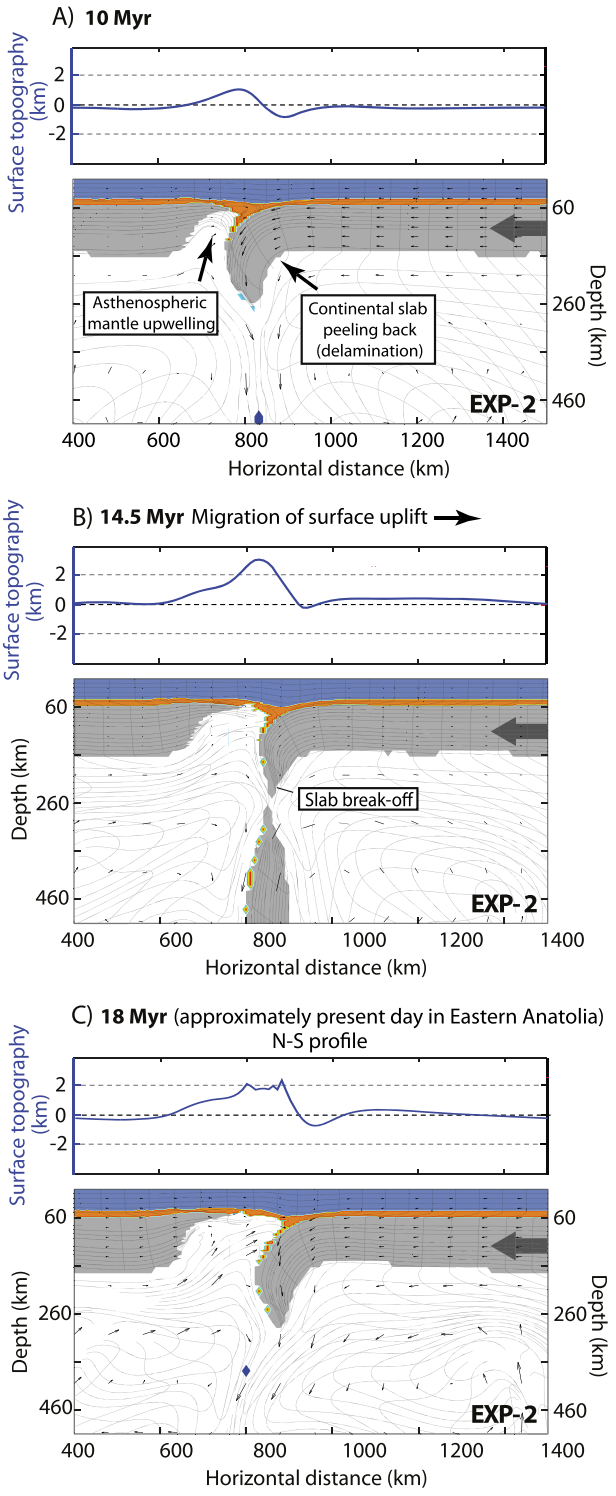

Figure 6. Geodynamic evolution of the reference/preferred experiment (EXP-2) demonstrating the continental lithosphere peel-back (delamination) and break-off from beneath the continental crust in Eastern Anatolia. These plots show such evolution at (a) 10, (b) 14.5, and (c) 18 Myr after the beginning of the experiment. The plots above the geodynamic model/lithospheric structure show the change in the thickness of the accretionary crust and surface topography plotted for each time, respectively.

$\sigma_y = 90$ MPa. For instance, at 18 Myr with the same model parameters, the slab break-off occurs under the continental lithosphere; however, this did not develop under oceanic lithosphere setting (see Figure 5b). It is because both the upper (wet quartzite) and lower crusts (felsic granulite) are more buoyant at continents to resist the downwelling of the negatively buoyant mantle lithosphere slab and this favors the vertical shearing, (therefore the break-off) between the crust and mantle lithosphere.

4. Summary of Experimental Results

So far, we discussed how modifications on model parameters control the surface and crustal evolution of a slab peeling process that occurs under oceanic and continental geological settings. In Figures 8b and 8c, with two diagrams (for ocean and continent) we demonstrate that there are certain linear relationships that exist between the model parameters and the evolution of the slab peeling/asthenospheric mantle replacement. Specifically, these diagrams represent the relation between the amounts of the following:

1. Slab peeling (S_p, plotted as the x axis),
2. Asthenospheric upwelling zone width beneath the crust (A_u, plotted as the y axis). (Please see schematic in Figure 8a that shows the corresponding variables at the x and y axes of these diagrams).

Both S_p and A_u are measured for the last phase of the experiments (18 Myr) with respect to their original position at 0 Myr. Namely, the slab-peeling amount (S_p) is calculated based on the final and initial positions of the hinge (Figure 8a):

$$S_p = D_{hf} - D_{hi} \tag{12}$$

D_{hi} is the initial decoupling hinge position that corresponds to the crust-slab decoupling point. D_{hi} is defined to where maximum crustal thickening occurs due to the slab pull (Figure 8a). D_{hf} indicates the final position of the hinge.

The peeling back slab yields mantle upwelling on both foreland (subducting) and hinterland (overriding) plates. Therefore, we suggest that A_u is also a function of the amount of displacement of (L_d) lithosphere asthenosphere boundary on the overriding (hinterland) plate in which the final position is L_{abf} and the original position is L_{abi}:

$$L_d = L_{abf} - L_{abi}. \tag{13}$$

Finally, the width of the asthenospheric upwelling zone is calculated as $A_u = S_p + L_d + G$, where G indicates the initial gap between two plates (constant for all experiments). These plots also include experimental predictions where the imposed plate convergence velocities (0, 1, 2 cm/year) and plastic yield stress of the descending slab (60, 75, 90, and 105 MPa) are varied.

There is a direct relationship between the strength, controlled by the plastic yield stress of the lithospheric slab, and how much it peels back (S_p), as well as the width of the asthenospheric upwelling zone (A_u). The experiments that have slabs with higher plastic yield stress (stronger) are more prone to retreat and peeling than that of lower yield strengths (softer). For example, if slab's yield stress is 105 MPa, it peels at least 50 km

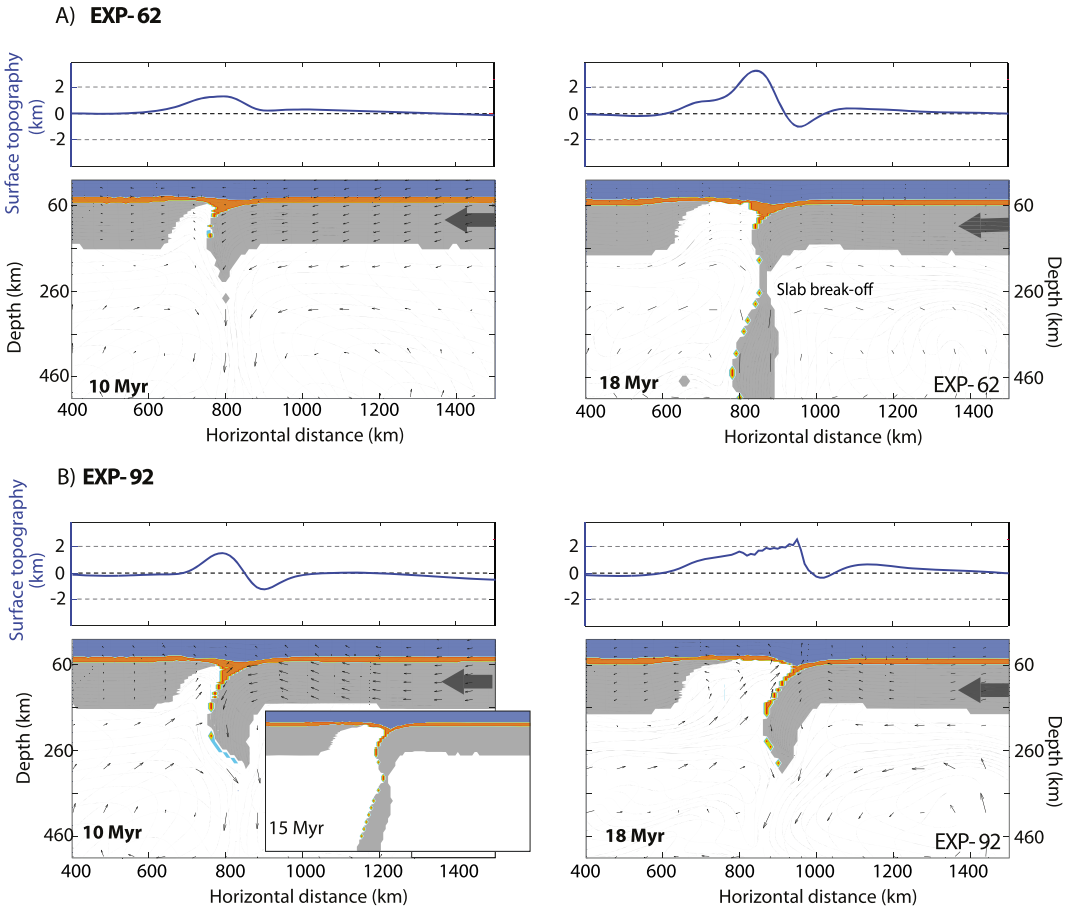

Figure 7. Geodynamic evolution of experiments; (a) EXP-62 and (b) EXP-92. The only difference between these two experiments is the plastic yield stress of the continental mantle lithosphere set initially as $\sigma_y = C_m$ (mantle). $\sigma_y = 60$ MPa of plastic yield stress is used for experiment EXP-62 (weaker rheology), while $\sigma_y = 90$ MPa is used for EXP-92 (stronger rheology). All other parameters are identical to the reference experiment (EXP-1). Both experiments show the model configuration for 10 and 18 Myr after the beginning of the experiment. Accordingly, surface topography profiles plots are shown on top of each panel for the relevant time frame.

more than the slab that has a plastic yield stress of 60 MPa. This is because relatively stronger slabs may not be subjected to break-off, or if they do, this happens during the later stages of the experiments. Instead, they generally tend to bend and lead to higher amount of hinge migration while subducting. Depending on when the initial slab break-off occurs, the models with lower lithospheric strength have delayed plate bending, and they subduct less and the related migration of the decoupling hinge (e.g., retreating hinge) is also relatively less. In a rarer case, for the experiment with 60 MPa yield stress and 2 cm/year plate velocity the slab does not peel back, but rather it moves forward toward the hinterland plate (i.e., an advancing trench motion for the slab).

The experiments for both ocean (Figure 8b) and continental (Figure 8c) rheological properties suggest that increasing plate convergence velocities are associated with a decreasing amount of slab peeling (S_p) and asthenospheric upwelling (A_u) (see supporting information Figures S1 and S2 for model results). With more plate shortening, the slab peeling process develops, but this is reduced since the lithospheric slab is continuously pushed against the overriding plate, similar to a plate subduction system. This may be an approximation to the incomplete/early stage collision/subduction where mantle lithospheres of these plates are not completely attached to each other, as has been suggested for various parts of the Mediterranean region (Royden, 1993). Specifically, the range of S_p varies from 250 to −30 km (advancing plate), and the plate convergence velocity of the lithosphere ranges between 0 and 2 cm/year. The slab peeling is suppressed (S_p) when the lithospheric plate is pushed at higher plate convergence velocities and this is also true for the amount of asthenospheric upwelling (A_u). Nevertheless, mantle upwelling zone and related positive

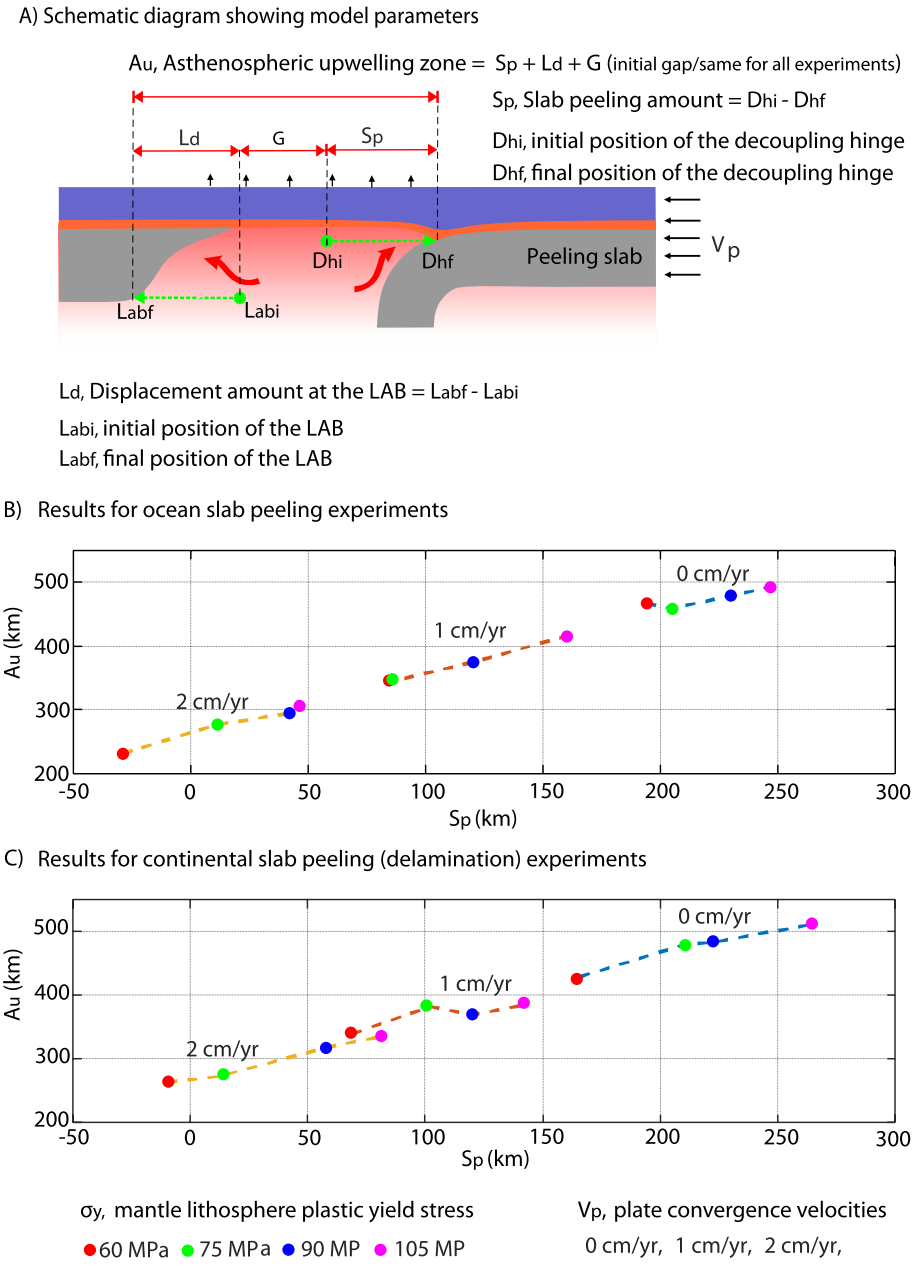

Figure 8. (a) Schematic 2-D diagram that shows the variables analyzed through slab peel-back experiments for both oceanic slab and the continental lithosphere. For example, measured distances between two points (A_u, asthenospheric upwelling zone, S_p, slab peeling amount) are demonstrated for the last time step (18 Myr after the beginning of the experiments). Detailed descriptions are explained in the text. The plot shows how such variable responds when plate convergence velocities and the plastic yield stress of the lithospheric slab vary for (b) ocean slab peeling experiments and (c) continental slab peeling (delamination) experiments.

surface elevation/plateau width may still be enlarged because active mantle upwelling under the crust as a response to slab removal is not purely single sided (asymmetric). Rather, the widening of the asthenospheric upwelling zone develops by the mantle flow entrainment on both beneath the plate where the slab peels back (foreland) and plate against to it (hinterland) (Figures 8b and 8c).

5. How Models Compare to the Uplift and Magmatism of Eastern Anatolia

In this section, we discuss how preferred ocean (EXP-1) and continental (EXP-2) lithosphere peel-back models might be agreeable to the tectonic evolution of Eastern Anatolia. Namely, we compare and contrast the

primary model predictions (e.g., 2-D profile/cross sections) against available geological and geophysical observables (N-S profile) cutting through the plateau.

First we compare the geodynamic configuration/slab-mantle interaction of EXP-1 and EXP-2 at 18 Myr (approximately present day), against seismic tomography models of the upper mantle and other geophysical studies (Figures 9a and 9b).

The model configuration for both EXP-1 and EXP-2 shows that the central section of the model domains in which lithospheric peel-back occurs are now occupied by asthenospheric mantle (Figure 9a). The relative widths of the asthenospheric mantle upwelling zone (A_u) are approximately 280 km for both models. Based on seismic tomography models, the lateral extent of the lower seismic velocity anomalies should be at least 300 km wide (from Bitlis Massif/suture zone to eastern Pontides/Lesser Caucasus) (Hearn & Ni, 1994; Sandvol et al., 2003; Al-Lazki et al., 2003; Piromallo & Morelli, 2003; Maggi & Priestley, 2005; Angus et al., 2006; Gök et al., 2007; Lei & Zhao, 2007; Zor, 2008; Özacar et al., 2008; Gök et al., 2011; Biryol et al., 2011; Mutlu & Karabulut, 2011; Koulakov et al., 2012; Bakırcı et al., 2012; Fichtner et al., 2013; Priestley & McKenzie, 2013; Skobeltsyn et al., 2014; Kind et al., 2015; Delph et al., 2015; Zabelina et al., 2016, Kaban et al., 2018; Portner et al., 2018). This has been interpreted as thinned lithosphere under the Eastern Anatolia, lying above hot asthenospheric mantle at depths shallower than 100 km. The presence of the asthenospheric mantle at shallow lithospheric depths has also been suggested by long-period magnetotelluric work in which low resistivity zones are interpreted as the localized pockets of fluid and melts in the lower crust that produced hot mantle uprising (Türkoğlu et al., 2008). Further, recent work by McNab et al. (2018) that interprets petrological and seismological data as well as long wavelength free-air gravity anomalies for Eastern Anatolia suggests that the surface elevation of the plateau is largely compensated by dynamic support induced by the asthenospheric mantle that resides under the crust.

Overall, the lithospheric structures of our numerical experimental results are comparable to the available observations (seismic tomography, Magnetotelluric data, gravity models) where the plateau does not have thick lithosphere; instead it is underlain by asthenospheric mantle at shallow depths.

In both sets of experiments, the slabs subduct steeply (>60° dip angle) where they are broken off at depths of 200–300 km. In EXP-1 where oceanic lithosphere has subducted, the portion of the detached slab exists within the model domain (200–500 km). However, in the continental peel-back/delamination experiments (EXP-2), such detached slab has entirely sunk deeper than 500 km as it does not appear in the model domain (Figure 9a). This suggests that the sinking rates of this detached slab is at the high end of the spectrum where various slab-sinking velocities are considered at depths of 0–410 km (Billen, 2010). In such case, while EXP-1 seems to be more agreeable for Eastern Anatolia's present-day lithospheric configuration, although it is hard to constrain this definitively since the tomography models by Lei and Zhao (2007), Zor (2008), Bakırcı et al. (2012), and Piromallo and Morelli (2003) suggest varying depths of slab break-off ranging from approximately 100–250 km (Figure 9b). Similarly there is relatively higher velocity anomaly at Biryol et al.'s (2011) seismic tomography model around the Bitlis suture zone, which may be used to interpret as a piece of detached slab. Recent tomography model by Portner et al. (2018) does not show slab break-off at shallow depths—as some tomography models do—although high velocity anomalies interpreted as slab fragments at depths of 400 and 800 km may be related with the of detached slabs. According to Lei and Zhao's (2007) model, the depth of slab break-off varies along the horizontal domain (along E-W, from 41°E-43°E). It can be inferred from both the regional and the large-scale *P* and *S* wave tomography studies that the fast, slab-like anomalies (i.e., slab fragments) are imaged in the upper mantle with different spatial localization. The detailed comparison of these seismic tomography models are out of our scope, yet, it should be noted that the controversial results in tomography models could be caused by the poor contrast of anomaly patterns in the upper mantle, data resolution and/or inversion techniques. Nevertheless, we interpret that both of our experiments are agreeable with the tomography models where slabs are detached. Having said that, here we are not biased toward any tomography model or even the slab break-off hypothesis that has allegedly occurred under the Eastern Anatolia. If it happened, models suggest such slab break-off most likely happened only a few million years ago (14.5 Myr model time) under Eastern Anatolia when reconciled with the seismic tomography model showing the present day position and depth of the detached slab. More importantly, one of the most important outcomes of this work is

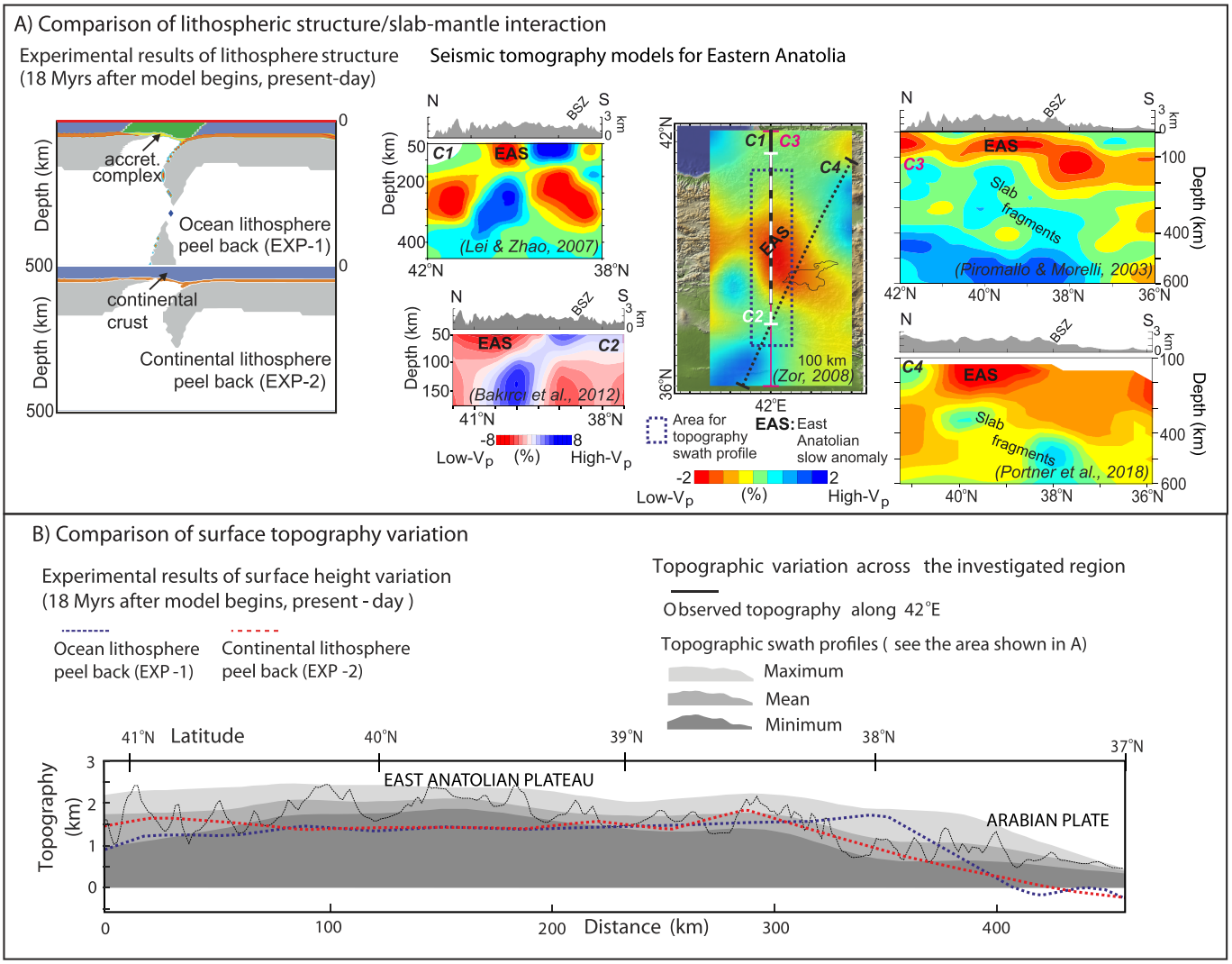

Figure 9. (a) Comparing the lithospheric configuration/slab-mantle interaction of the experimental results for the preferred experiments (EXP-1, EXP-2) against the N-S and NNE-SSW seismic tomography profiles across the East Anatolian Plateau (Bakırcı et al., 2012; Lei & Zhao, 2007; Piromallo & Morelli, 2003; Portner et al., 2018; Zor, 2008). (b) Comparing the surface topography variation of the experimental results for the preferred experiments (EXP-1, EXP-2) against the N-S topographic swath profiles across Eastern Anatolia.

that the slab break-off has an indiscernible role on the Eastern Anatolia's uplift and magmatism during the last 20 Myr where slab peel pack can account for such tectonic evolution.

In Figure 9b, we reconcile the topographic profiles of EXP-1 and EXP-2 (at 18 Myr, since the initiation of the experiments), against the mean elevation along the N-S topographic swath profiles (150 km wide region across Eastern Anatolia) (see inset map in Figure 9b for the area of the swath profile). Overall, when the lateral distance of the surface elevation along the plateau domain is scaled to 0.6, the model results reasonably well explain the surface uplift and elevation change (lowering) from the north portion of the plateau (2–1.5 km) to the Arabian plate (500 m). Due to the mantle uprising (as a response to lithospheric removal/peel-back) and the plate shortening, both experiments predict surface uplift of approximately 1.3–1.5 km in the middle section of the plateau in comparable time frame for the initiation of surface rise across East Anatolia (18 Myr). Though not uniform, such uplift amount and the timing is inferred from the surface exposure of Late Oligocene-Middle Miocene marine deposits (see section 1 and Figure 1b for stratigraphic sections) where their current elevations are ~ 1.5 km high above sea level. When the plateau center

(between $x = 100$ and 300 km) is taken as a reference distance for comparison between the model results against observed mean elevation, EXP-2 (with continental lithosphere rheology, shown in dashed red line) shows a more similar topographic trend in terms of the pattern and the magnitude on the plateau margins (for instance, between $x = 0$–100 km and $x = 250$–300 km). Nevertheless, such reconciliation along a selected profile may not reflect the change along the entire plateau.

In terms of geometry and structure, both experiments approximate the plateau type (e.g., southward tilting, flat top pattern), surface elevation consistent with Eastern Anatolia. Furthermore, there are rapid surface subsidences on the plate margin (till zero surface elevation) controlled by slab pull and this also comparable to the southward lowering (transient and migratory) elevation in the East Anatolian Plateau. We note that stratigraphic studies from Eastern Anatolia are in good agreement with (southward) migrating surface uplift, controlled by the peeling back of the lithospheric slab. Namely, by latest in the Early Miocene (23–16 Myr ago) the northern part of the plateau (e.g., Kağızman Tuzluca basin) was already above sea level (Metais et al., 2015; Şen et al., 2011; Varol et al., 2016), whereas the southern part (e.g., Muş-Van depression) emerged from the sea much later, during Serravalian (~13–11 Myr ago) (Demirtaşlı & Pisoni, 1965; Gelati, 1975; Sancay et al., 2006).

Corroborating the migration of surface, a compilation of age data from the igneous rocks suggests that there is southward younging magmatism in Eastern Anatolia during the last ~20 Myr (please see the supporting information Table S1 for the references). For instance, larger volumes of volcanic rocks around Lake Van-Muş area (Süphan, Nemrut, Tendürek, and Etrüsk) are less than 6 Myr old. In relation to this, our models predict that when the lithosphere peels off from the overlying crust, there is convective mantle circulation; therefore, heating and melting occurs at shallower depths beneath both the foreland (East Anatolia) and hinterland plates (Pontides, Lesser Caucasus in Armenia) (Sugden et al., 2019). Although the depth/distribution of the mantle flow varies (e.g., shallower/near crust under the foreland and deeper lithosphere under the hinterland), such processes can induce decompression related magmas (alkaline magmatism) under both the northern (e.g., Geghema highland Armenia) (Lebedev, Chernyshev, et al., 2013) and southern part of the plateau. This would serve as an alternative mechanism to small-scale convective instabilities and related melt production that may have operated under the Lesser Caucasus (Kaislaniemi et al., 2014; Neill et al., 2015). We note that the numerical experiments used in this work do not include formulations of thermopetrological properties of hydrous versus dry (decompression related) melt production; therefore, these results cannot be directly reconciled with the varying chemistry of magmatism in Eastern Anatolia (e.g., calc-alkaline to alkaline transition), while it helps to interpret the geodynamic origin (heating induced by mantle upwelling) for the volcanism and the surface (dynamic) uplift.

6. Conclusions

In this work, we use numerical experiments to explain how lithospheric (slab) peel-back from subduction-accretionary and continental crust and its potential break-off can drive surface uplift and subsidence variations in Eastern Anatolia. The model predictions for these two different types of crustal rheology are similar; therefore, results do not suggest whether the East Anatolian Plateau is made up of either type of crust. Nevertheless, compared against the geological, geophysical, and petrological observations, the model results are generally in accord with the tectonic evolution of the region during the last 18 Myr.

1. Slab peel-back from the crust can result in surface (plateau) uplift (~1.5 km high) and the zone of asthenospheric mantle upwelling (A_u) (~280 km wide). This "skinning" of the slab from the crust is similar to previously proposed "retreat tectonics" since the progressive slab removal controls the (southward) migration of the surface uplift and volcanism.
2. Sensitivity analyses for two important physical parameters (which are known to control the orogenesis) are conducted to investigate the (a) impact of the strength of the mantle lithosphere and (b) plate convergence velocities, on the evolution of slab peel-back and the related surface-crustal displacements. We find that the experiments with higher mantle lithosphere strength (plastic yield stresses) are associated with more slab peeling from the crust and wider asthenospheric upwelling zone (A_u). Meanwhile, when plate convergence velocities increase, slabs tend to peel back less, and consequently the asthenospheric upwelling zone and associated plateau becomes narrower.

3. During the evolution of the slab peeling/steepening, the break-off develops in the very last stage of the experiments (e.g., for the final 3 Myr), or in experiments with higher strength (e.g., ocean lithosphere model) the break-off does not occur during the 18 Myr of model evolution. For such timescale and wavelength, the models predict a very similar pattern and magnitude of surface topography profile with or without slab break-off and this suggests that slab break-off, if any, has an indiscernible role on the long-wavelength uplift of the entire plateau (from Bitlis Massif to Pontides/Lesser Caucasus). The last 20 Myr of magmatism in Eastern Anatolia can be accounted for heating of the lithosphere induced by mantle upwelling through such slab peel-back/removal mechanism without break off process.

Acknowledgments
Numerical calculations were done using a modified version of the SOPALE (2000) software. Phillip Fullsack at Dalhousie University originally developed the SOPALE modeling code with Chris Beaumont and his Geodynamics group. C. M., O. H. G., and M. K. acknowledge financial support from TUBITAK 3501 career programme (113Y200). R. P. acknowledges support from an NSERC Discovery Grant. E. Ş. U. thanks TUBITAK for the support by the 2219-International Postdoctoral Research Fellowship Programme. O. H. G. also acknowledges financial support from ITU BAP Project 41162 and young scientist (GEBİP) award from TUBA (Turkish Academy of Sciences). This work is based on numerical experiments where the "data" and the formulations used here can be reproduced by following the equations in the text. The numerical experiments presented here are available through contacting the authors. Meanwhile, documentation and the details for the numerical code can be found online (at http://geodynamics.oceanography.dal.ca/sopaledoc.html).

References

Açlan, M., & Altun, Y. (2018). Syn-collisional I-type Esenköy Pluton (Eastern Anatolia-Turkey): An indication for collision between Arabian and Eurasian plates. *Journal of African Earth Sciences*, *142*, 1–11. https://doi.org/10.1016/j.jafrearsci.2018.02.019

Afonso, J. C., G. Ranalli, & Fernandez, M. (2007). Density structure and buoyancy of the oceanic lithosphere revisited. *Geophysical Research Letters*, *34*, L10302. https://doi.org/10.1029/2007GL029515

Al-Lazki, A. I., Seber, D., Sandvol, E., Turkelli, N., Mohamad, R., & Barazangi, M. (2003). Tomographic Pn velocity and anisotropy structure beneath the Anatolian plateau (eastern Turkey) and the surrounding regions. *Geophysical Research Letters*, *30*(24), 8043. https://doi.org/10.1029/2003GL017391

Allen, M., Jackson, J., & Walker, R. (2004). Late Cenozoic reorganization of the Arabia-Eurasia collision and the comparison of short-term and long-term deformation rates. *Tectonics*, *23*, TC2008. https://doi.org/10.1029/2003TC001530

Angus, D. A., Wilson, D. C., Sandvol, E., & Ni, J. F. (2006). Lithospheric structure of the Arabian and Eurasian collision zone in eastern Turkey from *S*-wave receiver functions. *Geophysical Journal International*, *166*(3), 1335–1346. https://doi.org/10.1111/j.1365-246X.2006.03070.x

Ates, A., Bilim, F., & Buyuksarac, A. (2005). Curie point depth investigation of Central Anatolia, Turkey. *Pure and Applied Geophysics*, *162*(2), 357–371. https://doi.org/10.1007/s00024-004-2605-3

Bakırcı, T., Yoshizawa, K., & Özer, M. F. (2012). Three-dimensional *S*-wave structure of the upper mantle beneath Turkey from surface wave tomography. *Geophysical Journal International*, *190*(2), 1058–1076. https://doi.org/10.1111/j.1365-246X.2012.05526.x

Baratin, L. M., Mazzotti, S., Chéry, J., Vernant, P., Tahayt, A., & Mourabit, T. (2016). Incipient mantle delamination, active tectonics and crustal thickening in Northern Morocco: Insights from gravity data and numerical modeling. *Earth and Planetary Science Letters*, *454*, 113–120. https://doi.org/10.1016/j.epsl.2016.08.041

Beaumont, C., Ellis, S., Hamilton, J., & Fullsack, P. (1996). Mechanical model for subduction-collision tectonics of Alpine-type compressional orogens. *Geology*, *24*(8), 675–678. https://doi.org/10.1130/0091-7613(1996)024<0675:MMFSCT>2.3.CO;2

Beaumont, C., Nguyen, M. H., Jamieson, R. A., & Ellis, S. (2006). Crustal flow modes in large hot orogens. *Geological Society, London, Special Publications*, *268*(1), 91–145. https://doi.org/10.1144/GSL.SP.2006.268.01.05

Beck, S. L., Zandt, G., Ward, K. M., & Scire, A. (2015). Multiple styles and scales of lithospheric foundering beneath the Puna Plateau, central Andes. In DeCelles, P.G., Ducea, M.N., Carrapa, B., and Kapp, P.A. (Eds.), *Geodynamics of a cordilleran orogenic system: The Central Andes of Argentina and Northern Chile*, *Memoir* (Vol. 212. pp. 43–60). Boulder, CO: Geological Society of America. https://doi.org/10.1130/2015.1212(03)

Bigazzi, G., Yegingil, Z., Ercan, T., Oddone, M., & Özdoğan, M. (1997). Doğu Anadolu'daki obsidiyen içeren volkaniklerin "Fisyon Track" yöntemiyle yaş tayini (Age determination of obsidian bearing volcanics in eastern Anatolia using the fission-track dating method). *Geological Bulletin of Turkey*, *40*, 57–72.

Billen, M. I. (2010). Slab dynamics in the transition zone. *Physics of the Earth and Planetary Interiors*, *183*(1–2), 296–308. https://doi.org/10.1016/j.pepi.2010.05.005

Bird, P. (1979). Continental delamination and the Colorado Plateau. *Journal of Geophysical Research*, *84*(B13), 7561–7571. https://doi.org/10.1029/JB084iB13p07561

Biryol, B. C., Beck, S. L., Zandt, G., & Özacar, A. A. (2011). Segmented African lithosphere beneath the Anatolian region inferred from teleseismic *P*-wave tomography. *Geophysical Journal International*, *184*(3), 1037–1057. https://doi.org/10.1111/j.1365-246X.2010.04910.x

Bodur, Ö. F., GöğüŞ, O. H., Pysklywec, R. N., & Okay, A. I. (2018). Mantle lithosphere rheology, vertical tectonics, and the exhumation of (U)HP rocks. *Journal of Geophysical Research: Solid Earth*, *123*, 1824–1839. http://doi.org/10.1002/2017JB014546

Braun, J. (2010). The many surface expressions of mantle dynamics. *Nature Geoscience*, *3*(12), 825–833. https://doi.org/10.1038/ngeo1020

Burg, J. P. (2011). Rhodope: From Mesozoic convergence to Cenozoic extension. Review of petro-structural data in thegeochronological frame. In: (Eds.) Emmanuel Skourtsos and Gordon S. Lister. *Journal of the Virtual Explorer*, *42*, 1–44. https://doi.org/10.3809/jvirtex.2011.00270

Camp, V. E., & Hanan, B. B. (2008). A plume-triggered delamination origin for the Columbia River Basalt Group. *Geosphere*, *4*(3), 480–495. https://doi.org/10.1130/GES00175.1

Cavazza, W., Cattò, S., Zattin, M., Okay, A. I., & Reiners, P. (2018). Thermochronology of the Miocene Arabia-Eurasia collision zone of southeastern Turkey. *Geosphere*, *14*(5), 2277–2293. https://doi.org/10.1130/GES01637.1

Channell, J. E. T., & Mareschal, J. C. (1989). Delamination and asymmetric lithospheric thickening in the development of the Tyrrhenian Rift. *Geological Society, London, Special Publications*, *45*(1), 285–302. https://doi.org/10.1144/GSL.SP.1989.045.01.16

Chapman, J. B., Carrapa, B., Ballato, P., DeCelles, P. G., Worthington, J., Oimahmadov, I., et al. (2017). Intracontinental subduction beneath the Pamir Mountains: Constraints from thermokinematic modeling of shortening in the Tajik fold-and-thrust belt. *GSA Bulletin*, *129*(11-12), 1450–1471.

Chiarabba, C., & Chiodini, G. (2013). Continental delamination and mantle dynamics drive topography, extension and fluid discharge in the Apennines. *Geology*, *41*(6), 715–718. https://doi.org/10.1130/G33992.1

Chin, E. J., Lee, C. T. A., & Barnes, J. D. (2014). Thickening, refertilization, and the deep lithosphere filter in continental arcs: Constraints from major and trace elements and oxygen isotopes. *Earth and Planetary Science Letters*, *397*, 184–200. https://doi.org/10.1016/j.epsl.2014.04.022

Çolakoğlu, A. R., & Arehart, G. B. (2010). The petrogenesis of Sarıçimen (Çaldıran-Van) quartz monzodiorite: Implication for initiation of magmatism (Late Medial Miocene) in the east Anatolian collision zone, Turkey. *Lithos*, *119*(3-4), 607–620. https://doi.org/10.1016/j.lithos.2010.08.014

Copley, A., & Jackson, J. (2006). Active tectonics of the Turkish-Iranian plateau. *Tectonics*, *25*, TC6006. https://doi.org/10.1029/2005TC001906

Currie, C. A., Huismans, R. S., & Beaumont, C. (2008). Thinning of continental backarc lithosphere by flow-induced gravitational instability. *Earth and Planetary Science Letters*, *269*(3-4), 436–447. https://doi.org/10.1016/j.epsl.2008.02.037

Dahlen, F. A., Suppe, J., & Davis, D. (1984). Mechanics of fold-and-thrust belts and accretionary wedges: Cohesive Coulomb theory. *Journal of Geophysical Research*, *89*(B12), 10,087–10,101. https://doi.org/10.1029/JB089iB12p10087

Darold, A., & Humphreys, E. (2013). Upper mantle seismic structure beneath the Pacific Northwest: A plume-triggered delamination origin for the Columbia River flood basalt eruptions. *Earth and Planetary Science Letters*, *365*, 232–242. https://doi.org/10.1016/j.epsl.2013.01.024

Delph, J. R., Zandt, G., & Beck, S. L. (2015). A new approach to obtaining a 3D shear-wave velocity model of the crust and upper mantle: An application to eastern Turkey. *Tectonophysics*, *665*, 92–100. https://doi.org/10.1016/j.tecto.2015.09.031

Demir, T., Seyrek, A., Guillou, H., Scaillet, S., Westaway, R., & Bridgland, D. (2009). Preservation by basalt of a staircase of latest Pliocene terraces of the River Murat in eastern Turkey: Evidence for rapid uplift of the eastern Anatolian Plateau. *Global and Planetary Change*, *68*(4), 254–269. https://doi.org/10.1016/j.gloplacha.2009.02.008

Demirtaşlı, E., & Pisoni, C. (1965). The geology of Ahlat-Adilcevaz area (north of Lake Van). *Bulletin of The Mineral Research and Exploration*, *64*, 24–39.

Dewey, J. F., Hempton, M. R., Kidd, W. S. F., Saroglu, F. A. M. C., & Şengör, A. M. C. (1986). Shortening of continental lithosphere: The neotectonics of Eastern Anatolia—A young collision zone. *Geological Society, London, Special Publications*, *19*(1), 1–36. https://doi.org/10.1144/GSL.SP.1986.019.01.01

Di Giuseppe, P., Agostini, S., Lustrino, M., Karaoglu, Ö., SavaŞçin, M. Y., Manetti, P., & Ersoy, Y. (2017). Transition from compression to strike-slip tectonics revealed by Miocene-Pleistocene volcanism west of the Karliova triple junction (East Anatolia). *Journal of Petrology*, *58*(10), 2055–2087. https://doi.org/10.1093/petrology/egx082

Docherty, C., & Banda, E. (1995). Evidence for the eastward migration of the Alboran Sea based on regional subsidence analysis: A case for basin formation by delamination of the subcrustal lithosphere? *Tectonics*, *14*(4), 804–818. https://doi.org/10.1029/95TC00501

Elkins-Tanton, L. T. (2007). Continental magmatism, volatile recycling, and a heterogeneous mantle caused by lithospheric gravitational instabilities. *Journal of Geophysical Research*, *112*, B03405. https://doi.org/10.1029/2005JB004072

Ercan, T., Fujitami, T., Madsuda, J. L., Notsu, K., & Ui, T. (1990). Doğu ve Güneydoğu Anadolu Neojen-Kuvaterner volkanitlerine ilişkin yeni jeokjmyasal, radyometrik ve izotopik verilerin yorumu. *Maden Tetkik ve Arama Dergisi (Bull.Min.Res.Exp.)*, *110*(110), 143–164.

Erinç, S. (1953). Doğu Anadolu Coğrafyası (No. 572), İstanbul Üniversitesi Coğrafya Enstitüsü, [III] + 124 pp.

Farhoudi, G., & Karig, D. E. (1977). Makran of Iran and Pakistan as an active arc system. *Geology*, *5*(11), 664–668. https://doi.org/10.1130/0091-7613(1977)5<664:MOIAPA>2.0.CO;2

Fichtner, A., Trampert, J., Cupillard, P., Saygin, E., Taymaz, T., Capdeville, Y., & Villasenor, A. (2013). Multiscale full waveform inversion. *Geophysical Journal International*, *194*(1), 534–556. https://doi.org/10.1093/gji/ggt118

Fillerup, M. A., Knapp, J. H., Knapp, C. C., & Raileanu, V. (2010). Mantle earthquakes in the absence of subduction? Continental delamination in the Romanian Carpathians. *Lithosphere*, *2*(5), 333–340. https://doi.org/10.1130/L102.1

Fullsack, P. (1995). An arbitrary Lagrangian-Eulerian formulation for creeping flows and its application in tectonic models. *Geophysical Journal International*, *120*(1), 1–23. https://doi.org/10.1111/j.1365-246X.1995.tb05908.x

Gans, C. R., Beck, S. L., Zandt, G., Biryol, C. B., & Ozacar, A. A. (2009). Detecting the limit of slab break-off in central Turkey: New high-resolution Pn tomography results. *Geophysical Journal International*, *179*(3), 1566–1572. https://doi.org/10.1111/j.1365-246X.2009.04389.x

Gelati, R. (1975). Miocene marine sequence from Lake Van, Eastern Turkey. *Rivista Italiana di Paleontologia e Stratigrafia*, *81*, 477–490.

Girbacea, R., & Frisch, W. (1998). Slab in the wrong place: Lower lithospheric mantle delamination in the last stage of the Eastern Carpathian subduction retreat. *Geology*, *26*(7), 611–614. https://doi.org/10.1130/0091-7613(1998)026<0611:SITWPL>2.3.CO;2

Gleason, G. C., & Tullis, J. (1995). A flow law for dislocation creep of quartz aggregates determined with the molten salt cell. *Tectonophysics*, *247*(1-4), 1–23. https://doi.org/10.1016/0040-1951(95)00011-B

Göğüş, O. H., & Pysklywec, R. N. (2008a). Mantle lithosphere delamination driving plateau uplift and synconvergent extension in eastern Anatolia. *Geology*, *36*(9), 723–726. https://doi.org/10.1130/G24982A.1

Göğüş, O. H., & Pysklywec, R. N. (2008b). Near-surface diagnostics of dripping or delaminating lithosphere. *Journal of Geophysical Research*, *113*, B11404. https://doi.org/10.1029/2007JB005123

Göğüş, O. H., Pysklywec, R. N., Corbi, F., & Faccenna, C. (2011). The surface tectonics of mantle lithosphere delamination following ocean lithosphere subduction: Insights from physical-scaled analogue experiments. *Geochemistry, Geophysics, Geosystems*, *12*, Q05004. https://doi.org/10.1029/2010GC003430

Göğüş, O. H., Pysklywec, R. N., & Faccenna, C. (2016). Post-collisional lithospheric evolution of the Southeast Carpathians: Comparison of geodynamical models and observations. *Tectonics*, *35*, 1205–1224. https://doi.org/10.1002/2015TC004096

Göğüş, O. H., Pysklywec, R. N., & Faccenna, C. (2017). Geodynamical models for continental delamination and ocean lithosphere peel away in an orogenic setting. *Active Global Seismology: Neotectonics and Earthquake Potential of the Eastern Mediterranean Region*, *225*, 121. https://doi.org/10.1002/9781118944998

Göüş, O. H., Pysklywec, R. N., Şengör, A. M. C., & Gün, E. (2017). Drip tectonics and the enigmatic uplift of the Central Anatolian Plateau. *Nature Communications*, *8*(1), 1538. http://doi.org/10.1038/s41467-017-01611-3

Göğüş, O. H., & Ueda, K. (2018). Peeling back the lithosphere: Controlling parameters, surface expressions and the future directions in delamination modeling. *Journal of Geodynamics*, *117*, 21–40. https://doi.org/10.1016/j.jog.2018.03.003

Gök, R., Mellors, R. J., Sandvol, E., Pasyanos, M., Hauk, T., Takedatsu, R., & Javakishvirli, Z. (2011). Lithospheric velocity structure of the Anatolian plateau-Caucasus-Caspian region. *Journal of Geophysical Research*, *116*, B05303. https://doi.org/10.1029/2009JB000837

Gök, R., Pasyanos, M. E., & Zor, E. (2007). Lithospheric structure of the continent–continent collision zone: Eastern Turkey. *Geophysical Journal International*, *169*(3), 1079–1088. https://doi.org/10.1111/j.1365-246X.2006.03288.x

Gray, R., & Pysklywec, R. N. (2012). Geodynamic models of mature continental collision: Evolution of an orogen from lithospheric subduction to continental retreat/delamination. *Journal of Geophysical Research*, *117*, B03408. https://doi.org/10.1029/2011JB008692

Hearn, T. M., & Ni, J. F. (1994). Pn velocities beneath continental collision zones: The Turkish-Iranian Plateau. *Geophysical Journal International*, *117*(2), 273–283. https://doi.org/10.1111/j.1365-246X.1994.tb03931.x

Hirth, G., & Kohlstedt, D. L. (1996). Water in the oceanic upper mantle: Implications for rheology, melt extraction and the evolution of the lithosphere. *Earth and Planetary Science Letters*, *144*(1-2), 93–108. https://doi.org/10.1016/0012-821X(96)00154-9

Houseman, G. A., McKenzie, D. P., & Molnar, P. (1981). Convective instability of a thickened boundary layer and its relevance for the thermal evolution of continental convergent belts. *Journal of Geophysical Research*, *86*(B7), 6115–6132. https://doi.org/10.1029/JB086iB07p06115

Hubert-Ferrari, A., King, G., van der Woerd, J., Villa, I., Altunel, E., & Armijo, R. (2009). Long-term evolution of the North Anatolian Fault: New constraints from its eastern termination. In D. J. J. van Hinsbergen, et al. (Eds.), *Collision and collapse at the Africa-Arabia-Eurasia subduction zone*, *Special Publication* (Vol. 311, pp. 133–154). London: Geological Society. https://doi.org/10.1144/SP311.5

Huismans, R. S., & Beaumont, C. (2008). Complex rifted continental margins explained by dynamical models of depth-dependent lithospheric extension. *Geology*, *36*(2), 163–166. https://doi.org/10.1130/G24231A.1

Innocenti, F., Mazzuoli, R., Pasquare, G., Di Brozolo, F. R., & Villari, L. (1976). Evolution of the volcanism in the area of interaction between the Arabian, Anatolian and Iranian plates (Lake Van, Eastern Turkey). *Journal of Volcanology and Geothermal Research*, *1*(2), 103–112. https://doi.org/10.1016/0377-0273(76)90001-9

Innocenti, F., Mazzuoli, R., Pasquare, G., Di Brozolo, F. R., & Villari, L. (1982). Tertiary and quaternary volcanism of the Erzurumkars area (Eastern Turkey): Geochronological data and geodynamic evolution. *Journal of Volcanology and Geothermal Research*, *13*(3-4), 223–240. https://doi.org/10.1016/0377-0273(82)90052-X

Innocenti, F., Mazzuoli, R., Pasquare, G., Serri, G., & Villari, L. (1980). Geology of the volcanic area north of Lake Van (Turkey). *Geologische Rundschau*, *69*(1), 292–323. https://doi.org/10.1007/BF01869038

Kaban, M. K., Petrunin, A. G., El Khrepy, S., & Al-Arifi, N. (2018). Diverse continental subduction scenarios along the Arabia-Eurasia collision zone. *Geophysical Research Letters*, *45*, 6898–6906. https://doi.org/10.1029/2018GL078074

Kaislaniemi, L., Van Hunen, J., Allen, M. B., & Neill, I. (2014). Sublithospheric small-scale convection—A mechanism for collision zone magmatism. *Geology*, *42*(4), 291–294. https://doi.org/10.1130/G35193.1

Keskin, M. (2003). Magma generation by slab steepening and breakoff beneath a subduction-accretion complex: An alternative model for collision-related volcanism in Eastern Anatolia, Turkey. *Geophysical Research Letters*, *30*(24), 8046. https://doi.org/10.1029/2003GL018019

Keskin, M. (2007). Eastern Anatolia: A hotspot in a collision zone without a mantle plume. In G. R. Foulger & D. M. Jurdy (Eds.), *Plates, plumes, and planetary processes: Geological Society of America Special Paper* (Vol. 430, pp. 693–722). https://doi.org/10.1130/2007.2430(32)

Keskin, M., Pearce, J. A., & Mitchell, J. G. (1998). Volcano-stratigraphy and geochemistry of collision-related volcanism on the Erzurum–Kars Plateau, northeastern Turkey. *Journal of Volcanology and Geothermal Research*, *85*(1-4), 355–404. https://doi.org/10.1016/S0377-0273(98)00063-8

Kheirkhah, M., Allen, M. B., & Emami, M. (2009). Quaternary syn-collision magmatism from the Iran/Turkey borderlands. *Journal of Volcanology and Geothermal Research*, *182*(1-2), 1–12. https://doi.org/10.1016/j.jvolgeores.2009.01.026

Kimura, G., & Ludden, J. (1995). Peeling oceanic crust in subduction zones. *Geology*, *23*(3), 217–220. https://doi.org/10.1130/0091-7613(1995)023b0217:POCISZN2.3.CO;2

Kind, R., Eken, T., Tilmann, F., Sodoudi, F., Taymaz, T., Bulut, F., et al. (2015). Thickness of the lithosphere beneath Turkey and surroundings from *S*-receiver functions. *Solid Earth*, *6*(3), 971–984. https://doi.org/10.5194/se-6-971-2015

Koulakov, I., Zabelina, I., Amanatashvili, I., & Meskhia, V. (2012). Nature of orogenesis and volcanism in the Caucasus region based on results of regional tomography. *Solid Earth*, *3*(2), 327–337. https://doi.org/10.5194/se-3-327-2012

Le Pourhiet, L., Gurnis, M., & Saleeby, J. (2006). Mantle instability beneath the Sierra Nevada mountains in California and Death Valley extension. *Earth and Planetary Science Letters*, *251*(1-2), 104–119. https://doi.org/10.1016/j.epsl.2006.08.028

Le Roux, V., Bodinier, J. L., Tommasi, A., Alard, O., Dautria, J. M., Vauchez, A., & Riches, A. J. V. (2007). The Lherz spinel lherzolite: Refertilised rather than pristine mantle. *Earth and Planetary Science Letters*, *259*(3-4), 599–612. https://doi.org/10.1016/j.epsl.2007.05.026

Lebedev, V. A., Chernyshev, I. V., Shatagin, K. N., Bubnov, S. N., & Yakushev, A. I. (2013). Geochronology, isotope Sr Nd characteristics and origin of Quaternary volcanic rocks within Geghama highland (Lesser Caucasus, Armenia). *Journal of Volcanology and Seismology*, *8*(2), 93–107. https://doi.org/10.1134/S0742046314020043

Lebedev, V. A., Chugaev, A. V., Ünal, E., Sharkov, E. V., & Keskin, M. (2016). Late Pleistocene Tendurek volcano (Eastern Anatolia, Turkey). 2. Geochemistry and petrogenesis of the rocks. 2. Geochemistry and petrogenesis of the rocks. *Petrology*, *24*(3), 234–270. https://doi.org/10.1134/S0869591116030043

Lebedev, V. A., Parfenov, A. V., & Yakushev, A. I. (2018). Neogene–Quaternary magmatism of the Çaldıran plain and its vicinity (Eastern Turkey): An example of post-collisional transition from subduction to intraplate type. *Petrology*, *26*(5), 469–491. https://doi.org/10.1134/S0869591118050053

Lebedev, V. A., Sharkov, E. V., Keskin, M., & Oyan, V. (2010). Geochronology of Late Cenozoic volcanism in the area of Van Lake, Turkey: An example of development dynamics for magmatic processes. *Doklady Earth Sciences*, *433*(2), 1031–1037. https://doi.org/10.1134/S1028334X1008009X

Lebedev, V. A., Sharkov, E. V., Ünal, E., & Keskin, M. (2016). Late pleistocene Tendürek volcano (Eastern Anatolia, Turkey): I. Geochronology and petrographic characteristics of igneous rocks. *Petrology*, *24*(2), 127–152. https://doi.org/10.1134/S0869591116020041

Lebedev, V. A., Volkov, V. N., Sagatelyan, A. K., & Chernyshev, I. V. (2013). Spatial migration of magmatic activity within the Caucasian segment of the Alpine belt in the early neogene under the conditions of geotectonic setting change: Isotope-geochronological data. *Doklady Earth Sciences*, *448*(2), 225–231. https://doi.org/10.1134/S1028334X13020141

Leech, M. L. (2001). Arrested orogenic development: Eclogitization, delamination, and tectonic collapse. *Earth and Planetary Science Letters*, *185*(1-2), 149–159. https://doi.org/10.1016/S0012-821X(00)00374-5

Lei, J., & Zhao, D. (2007). Teleseismic evidence for a break-off subducting slab under Eastern Turkey. *Earth and Planetary Science Letters*, *257*(1-2), 14–28. https://doi.org/10.1016/j.epsl.2007.02.011

Levander, A., Schmandt, B., Miller, M. S., Liu, K., Karlstrom, K. E., Crow, R. S., & Humphreys, E. D. (2011). Continuing Colorado plateau uplift by delamination-style convective lithospheric downwelling. *Nature*, *472*(7344), 461–465. https://doi.org/10.1038/nature10001

Mackwell, S. J., Zimmerman, M. E., & Kohlstedt, D. L. (1998). High-temperature deformation of dry diabase with application to tectonics on Venus. *Journal of Geophysical Research*, *103*(B1), 975–984. https://doi.org/10.1029/97JB02671

Maggi, A., & Priestley, K. (2005). Surface waveform tomography of the Turkish–Iranian plateau. *Geophysical Journal International*, *160*(3), 1068–1080. https://doi.org/10.1111/j.1365-246X.2005.02505.x

McNab, F., Ball, P. W., Hoggard, M. J., & White, N. J. (2018). Neogene uplift and magmatism of Anatolia: Insights from drainage analysis and basaltic geochemistry. *Geochemistry, Geophysics, Geosystems*, *19*(1), 175–213. https://doi.org/10.1002/2017GC007251

Metais, G., Sen, S., Sözeri, K., Peigné, S., & Varol, B. (2015). Late Paleogene terrestrial fauna and paleoenvironments in Eastern Anatolia: New insights from the Kağızman-Tuzluca Basin. *Journal of Asian Earth Sciences*, *107*, 96–109. https://doi.org/10.1016/j.jseaes.2015.03.048

Mohammadi, A., Burg, J. P., Winkler, W., Ruh, J., & von Quadt, A. (2016). Detrital zircon and provenance analysis of Late Cretaceous–Miocene onshore Iranian Makran strata: Implications for the tectonic setting. *Bulletin*, *128*(9-10), 1481–1499. https://doi.org/10.1130/B31361.1

Molnar, P., England, P., & Martinod, J. (1993). Mantle dynamics, uplift of the Tibetan Plateau, and the Indian monsoon. *Reviews of Geophysics*, *31*(4), 357–396. https://doi.org/10.1029/93RG02030

Mutlu, A. K., & Karabulut, H. (2011). Anisotropic Pn tomography of Turkey and adjacent regions. *Geophysical Journal International*, *187*(3), 1743–1758. https://doi.org/10.1111/j.1365-246X.2011.05235.x

Neill, I., Meliksetian, K., Allen, M. B., Navarsdyan, G., & Klaudia, K. (2015). Petrogenesis of mafic collision zone magmatism: The Armenian sector of the Turkish-Iranian Plateau. *Chemical Geology*, *403*, 24–41. https://doi.org/10.1016/j.chemgeo.2015.03.013

Notsu, K., Fujitani, T., Ui, T., Matsuda, J., & Ercan, T. (1995). Geochemical features of collision-related volcanic rocks in central and eastern Anatolia, Turkey. *Journal of Volcanology and Geothermal Research*, *64*(3-4), 171–191. https://doi.org/10.1016/0377-0273(94)00077-T

Okay, A. I., & Şahintürk, Ö. (1997). Geology of the eastern Pontides. In A. G. Robinson (Ed.), *Regional and petroleum geology of the Black Sea and surrounding region* (Vol. 68, pp. 291–311). Tulsa, OK: American Association of Petroleum Geologists Memoir.

Okay, A. I., Zattin, M., & Cavazza, W. (2010). Apatite fission-track data for the Miocene Arabia-Eurasia collision. *Geology*, *38*(1), 35–38. https://doi.org/10.1130/G30234.1

Oyan, V. (2018). Ar-Ar dating and petrogenesis of the Early Miocene TaŞkapı-Mecitli (ErciŞ-Van) granitoid, Eastern Anatolia Collisional Zone, Turkey. *Journal of Asian Earth Sciences*, *158*, 210–226. https://doi.org/10.1016/j.jseaes.2018.03.002

Oyan, V., Keskin, M., Lebedev, V. A., Chugaev, A. V., & Sharkov, E. V. (2016). Magmatic evolution of the Early Pliocene Etrüsk strato-volcano, eastern Anatolian collision zone, Turkey. *Lithos*, *256-257*, 88–108. http://doi.org/10.1016/j.lithos.2016.03.017

Oyan, V., Keskin, M., Lebedev, V. A., Chugaev, A. V., Sharkov, E. V., & Ünal, E. (2017). Petrology and geochemistry of the Quaternary mafic volcanism to the NE of Lake Van, Eastern Anatolian Collision Zone, Turkey. *Journal of Petrology*, *58*(9), 1701–1728. https://doi.org/10.1093/petrology/egx070

Özacar, A. A., Gilbert, H., & Zandt, G. (2008). Upper mantle discontinuity structure beneath East Anatolian Plateau (Turkey) from receiver functions. *Earth and Planetary Science Letters*, *269*(3-4), 427–435. https://doi.org/10.1016/j.epsl.2008.02.036

Özcan, E., Less, G., Báldi-Beke, M., & Kollányi, K. (2010). Oligocene hyaline larger foraminifera from KelereŞdere Section (MuŞ, Eastern Turkey). *Micropaleontology*, 465–493.

Özdemir, Y. (2011) Volcanostratigraphy and petrogenesis of Süphan Stratovolcano: METU-Middle East Technical University. Unpublished PhD thesis.

Özdemir, Y., & Güleç, N. (2014). Geological and geochemical evolution of the Quaternary Süphan Stratovolcano, Eastern Anatolia, Turkey: Evidence for the lithosphere–asthenosphere interaction in post-collisional volcanism. *Journal of Petrology*, *55*(1), 37–62. https://doi.org/10.1093/petrology/egt060

Özdemir, Y., Karaoğlu, O., Tolluoğlu, A. U., & Güleç, N. (2006). Volcano-stratigraphy and petrogenesis of the Nemrut stratovolcano (East Anatolian High Plateau): The most recent post collisional volcanism in Turkey. *Chemical Geology*, *226*(3–4), 189–211. https://doi.org/10.1016/j.chemgeo.2005.09.020

Pearce, J. A., Bender, J. F., De Long, S. E., Kidd, W. S. F., Low, P. J., Güner, Y., et al. (1990). Genesis of collision volcanism in Eastern Anatolia, Turkey. *Journal of Volcanology and Geothermal Research*, *44*(1-2), 189–229. https://doi.org/10.1016/0377-0273(90)90018-B

Piromallo, C., & Morelli, A. (2003). *P* wave tomography of the mantle under the Alpine-Mediterranean area. *Journal of Geophysical Research*, *108*(B2), 2065. https://doi.org/10.1029/2002JB001757

Platt, J. P., Leggett, J. K., Young, J., Raza, H., & Alam, S. (1985). Large-scale sediment underplating in the Makran accretionary prism, southwest Pakistan. *Geology*, *13*(7), 507–511. https://doi.org/10.1130/0091-7613(1985)13<507:LSUITM>2.0.CO;2

Portner, D. E., Delph, J. R., Biryol, C. B., Beck, S. L., Zandt, G., Özacar, A. A., et al. (2018). Subduction termination through progressive slab deformation across Eastern Mediterranean subduction zones from updated *P*-wave tomography beneath Anatolia. *Geosphere*, *14*(3), 907–925. https://doi.org/10.1130/GES01617.1

Priestley, K., & McKenzie, D. (2013). The relationship between shear wave velocity, temperature, attenuation and viscosity in the shallow part of the mantle. *Earth and Planetary Science Letters*, *381*, 78–91. https://doi.org/10.1016/j.epsl.2013.08.022

Pysklywec, R. N., Beaumont, C., & Fullsack, P. (2002). Lithospheric deformation during the early stages of continental collision: Numerical experiments and comparison with South Island, New Zealand. *Journal of Geophysical Research*, *107*(B7), 2133. https://doi.org/10.1029/2001JB000252

Pysklywec, R. N., Göğüş, O., Percival, J., Cruden, A. R., & Beaumont, C. (2010). Insights from geodynamical modeling on possible fates of continental mantle lithosphere: Collision, removal, and overturn. *Canadian Journal of Earth Sciences*, *47*(4), 541–563. https://doi.org/10.1139/E09-043

Rabayrol, F., Hart, C. J. R., & Thorkelson, D. J. (2019). Temporal, spatial, geochemical evolution of late Cenozoic post subduction magmatism in central and eastern Anatolia, Turkey. *Lithos*, *336*, 67–96. https://doi.org/10.1016/j.lithos.2019.03.022

Ranalli, G. (1997). Rheology of the lithosphere in space and time. *Geological Society, London, Special Publications*, *121*(1), 19–37. https://doi.org/10.1144/GSL.SP.1997.121.01.02

Reilinger, R., McClusky, S., Vernant, P., Lawrence, S., Ergintav, S., Cakmak, R., et al. (2006). GPS constraints on continental deformation in the Africa-Arabia-Eurasia continental collision zone and implications for the dynamics of plate interactions. *Journal of Geophysical Research*, *111*, B05411. https://doi.org/10.1029/2005JB004051

Royden, L. H. (1993). The tectonic expression slab pull at continental convergent boundaries. *Tectonics*, *12*(2), 303–325. https://doi.org/10.1029/92TC02248

Ryan, W. B. F., Carbotte, S. M., Coplan, J. O., O'Hara, S., Melkonian, A., Arko, R., et al. (2009). Global multi-resolution topography-synthesis. *Geochemistry, Geophysics, Geosystems*, *10*, Q03014. https://doi.org/10.1029/2008GC002332

Saleeby, J., Le Pourhiet, L., Saleeby, Z., & Gurnis, M. (2012). Epeirogenic transients related to mantle lithosphere removal in the southern Sierra Nevada region, California, part I: Implications of thermomechanical modeling. *Geosphere*, *8*(6), 1286–1309. https://doi.org/10.1130/GES00746.1

Saleeby, J., Saleeby, Z., & Le Pourhiet, L. (2013). Epeirogenic transients related to mantle lithosphere removal in the southern Sierra Nevada region, California: Part II. Implications of rock uplift and basin subsidence relations. *Geosphere*, *9*(3), 394–425. https://doi.org/10.1130/GES00816.1

Sancay, R. H., Bati, Z., Işik, U., Kirici, S., & Akca, N. (2006). Palynomorph, foraminifera, and calcareous nannoplankton biostratigraphy of Oligo–Miocene sediments in the Muş Basin, Eastern Anatolia, Turkey. *Turkish Journal of Earth Sciences*, *15*(3), 259–319.

Sandvol, E., Turkelli, N., & Barazangi, M. (2003). The Eastern Turkey Seismic Experiment: The study of a young continent-continent collision. *Geophysical Research Letters*, *30*(24), 8038. https://doi.org/10.1029/2003GL018912

Şaroğlu, F., & Yılmaz, Y. (1987). Geological evolution and basin models during neotectonic episode in the eastern Anatolia. *Maden Tetkik ve Arama Dergisi Bulletin of The Mineral Research and Exploratio*, *107*, 61–83.

Schleiffarth, W., Darin, M., Umhoefer, P., & Reid, R. M. (2018). Dynamics of episodic Late Cretaceous–Cenozoic magmatism across Central to Eastern Anatolia: New insights from an extensive geochronology compilation. *Geosphere*, *14*(5), 1990–2008. https://doi.org/10.1130/GES01647.1

Schubert, G., Turcotte, D. L., & Olson, P. (2001). *Mantle convection in the Earth and planets*. Cambridge: Cambridge University Press.

Selçuk, A. S., Erturaç, M. K., & Nomade, S. (2016). Geology of the Çaldıran fault, Eastern Turkey: age, slip rate and implications on the characteristic slip behaviour. *Tectonophysics*, *680*, 155–173. https://doi.org/10.1016/j.tecto.2016.05.019

Şen, P. A., Temel, A., & Gourgaud, A. (2004). Petrogenetic modelling of Quaternary post-collisional volcanism: A case study of central and eastern Anatolia. *Geological Magazine*, *141*(1), 81–98. https://doi.org/10.1017/S0016756803008550

Şen, S., Antoine, P. O., Varol, B., Ayyildiz, T., & Sözeri, K. (2011). Giant rhinoceros *Paraceratherium* and other vertebrates from Oligocene and middle Miocene deposits of the Kağızman-Tuzluca Basin, Eastern Turkey. *Naturwissenschaften*, *98*(5), 407–423. https://doi.org/10.1007/s00114-011-0786-z

Şengör, A. C., Özeren, M. S., Keskin, M., Sakınç, M., Özbakır, A. D., & Kayan, I. (2008). Eastern Turkish high plateau as a small Turkic-type orogen: Implications for post-collisional crust-forming processes in Turkic-type orogens. *Earth-Science Reviews*, *90*(1-2), 1–48. https://doi.org/10.1016/j.earscirev.2008.05.002

Şengör, A. M. C., & Kidd, W. S. F. (1979). Post-collisional tectonics of the Turkish-Iranian plateau and a comparison with Tibet. *Tectonophysics*, *55*(3-4), 361–376. https://doi.org/10.1016/0040-1951(79)90184-7

Şengör, A. M. C., Özeren, S., Genç, T., & Zor, E. (2003). East Anatolian high plateau as a mantle-supported, north-south shortened domal structure. *Geophysical Research Letters*, *30*(24), 8045. https://doi.org/10.1029/2003GL017858

Şengör, A. M. C., & Yılmaz, Y. (1981). Tethyan evolution of Turkey: A plate tectonic approach. *Tectonophysics*, *75*(3-4), 181–241. https://doi.org/10.1016/0040-1951(81)90275-4

Şengül Uluocak, E., Pysklywec, R. N., Göğüş, O. H., & Ulugergerli, E. U. (2019). Multi-dimensional geodynamic modeling in the southeast Carpathians: Upper mantle flow induced surface topography anomalies. *Geochemistry, Geophysics, Geosystems*, *20*(7), 3134–3149. https://doi.org/10.1029/2019GC008277

Skobeltsyn, G., Mellors, R., Gök, R., Türkelli, N., Yetirmishli, G., & Sandvol, E. (2014). Upper mantle *S* wave velocity structure of the East Anatolian-Caucasus region. *Tectonics*, *33*, 207–221. https://doi.org/10.1002/2013TC003334

Stern, T., Houseman, G., Salmon, M., & Evans, L. (2013). Instability of a lithospheric step beneath western North Island, New Zealand. *Geology*, *41*(4), 423–426. https://doi.org/10.1130/G34028.1

Sugden, P. J., Savov, I. P., Wilson, M., Meliksetian, K., Navasardyan, G., & Halama, R. (2019). The thickness of the mantle lithosphere and collision-related volcanism in the lesser Caucasus. *Journal of Petrology*, *60*(2), 199–230. https://doi.org/10.1093/petrology/egy111

Sumita, M., & Schmincke, H.-U. (2013). Impact of volcanism on the evolution of Lake Van II: Temporal evolution of explosive volcanism of Nemrut Volcano (eastern Anatolia) during the past ca. 0.4 Ma. *Journal of Volcanology and Geothermal Research*, *253*, 15–34. https://doi.org/10.1016/j.jvolgeores.2012.12.009

Tezcan, A. K. (1995). Geothermal explorations and heat flow in Turkey. In M. L. Gupta, & M. Yamano (Eds.), *Terrestrial Heat Flow and Geothermal Energy in Asia* (pp. 23–42). Oxford: Oxford and IBH.

Topuz, G., Okay, A. I., Altherr, R., Schwarz, W. H., Siebel, W., Zack, T., et al. (2011). Post-collisional adakite-like magmatism in the Ağvanis Massif and implications for the evolution of the Eocene magmatism in the Eastern Pontides (NE Turkey). *Lithos*, *125*(1-2), 131–150. https://doi.org/10.1016/j.lithos.2011.02.003

Türkoğlu, E., Unsworth, M., Çağlar, İ., Tuncer, V., & Avşar, Ü. (2008). Lithospheric structure of the Arabia-Eurasia collision zone in eastern Anatolia: Magnetotelluric evidence for widespread weakening by fluids? *Geology*, *36*(8), 619–622. https://doi.org/10.1130/G24683A.1

Valera, J. L., Negredo, A. M., & Villaseñor, A. (2008). Asymmetric delamination and convective removal numerical modeling: Comparison with evolutionary models for the Alboran Sea region. *Pure and Applied Geophysics*, *165*(8), 1683–1706. https://doi.org/10.1007/s00024-008-0395-8

van Wyk de Vries, B., Byrne, P., Delcamp, A., Einarson, P., Göğüş, O., Guilbaud, M.-N., et al. (2018). A global framework for the Earth: Putting geological sciences in context. *Global and Planetary Change*. https://doi.org/10.1016/j.gloplacha.2017.12.019

Varol, B., Şen, Ş., Ayyildiz, T., Sözeri, K., Karakas, Z., & Métais, G. (2016). Sedimentology and stratigraphy of Cenozoic deposits in the Kağızman-Tuzluca Basin, northeastern Turkey. *International Journal of Earth Sciences*, *105*(1), 107–137. https://doi.org/10.1007/s00531-015-1201-3

von Huene, R., & Scholl, D. W. (1991). Observations at convergent margin concerning sediment subduction, subduction erosion and the growth of the continental crust. *Reviews of Geophysics*, *29*(3), 279–316. https://doi.org/10.1029/91RG00969

Wang, H., & Currie, C. A. (2015). Magmatic expression of continental lithosphere removal. *Journal of Geophysical Research: Solid Earth*, *120*, 7239–7260. https://doi.org/10.1002/2015JB012112

Yan, Q. Z., & Mechie, J. (1989). A fine structural section through the crust and lower lithosphere along the axial region of the Alps. *Geophysical Journal International*, *98*(3), 465–488. https://doi.org/10.1111/j.1365-246X.1989.tb02284.x

Yılmaz, A., & Yılmaz, H. (2019). Structural evolution of the Eastern Anatolian Basins: An example from collisional to postcollisional tectonic processes, Turkey. *Turkish Journal of Earth Sciences*, *28*(3), 329–350. https://doi.org/10.3906/yer-1805-20

Yılmaz, Y. (1990). Comparison of young volcanic associations of western and eastern Anatolia formed under a compressional regime: A review. *Journal of Volcanology and Geothermal Research*, *44*(1-2), 69–87. https://doi.org/10.1016/0377-0273(90)90012-5

Yılmaz, Y., Yiğitbaş, E., & Genç, Ş. C. (1993). Ophiolitic and metamorphic assemblages of southeast Anatolia and their significance in the geological evolution of the orogenic belt. *Tectonics*, *12*(5), 1280–1297. https://doi.org/10.1029/93TC00597

Zabelina, I., Koulakov, I., Amanatashvili, I., El Khrepy, S., & Al-Arifi, N. (2016). Seismic structure of the crust and uppermost mantle beneath Caucasus based on regional earthquake tomography. *Journal of Asian Earth Sciences*, *119*, 87–99. https://doi.org/10.1016/j.jseaes.2016.01.010

Zor, E. (2008). Tomographic evidence of slab detachment beneath eastern Turkey and the Caucasus. *Geophysical Journal International*, *175*(3), 1273–1282. https://doi.org/10.1111/j.1365-246X.2008.03946.x